Petrophysical Properties of Deformed Sandstone Reservoir

Saeideh Shekari-Namin

Master's Thesis in Petroleum Geology

Department of Earth science
&
Centre for Integrated Petroleum Research

Faculty of Mathematics and Natural Science

University of Bergen 2012

Acknowledgement

This thesis was completed as a part of the Master degree programme at the department of Earth Science and Centre of Integrated Petroleum Research (CIPR) at the University of Bergen. The work was part of the IMPACT Project supported by Statoil and the Research Council of Norway.

At the first place, I am grateful to my supervisor, Anita Torabi for her maintained support and supervision during the thesis work and also to my co-supervisors Arne Skauge, Christian Hermanrud and Eivind Bastesen for their useful guidance.

Special thanks go to Bartek Florczyk Vik for his comprehensive guidance and help in experimental part of thesis and helpful comments. I am also thankful for help that I received from Per Arne Ormehaug during experiments.

Finally I would like to express my thanks and love to my family, specially my dears Hesam and Selin for all their care and strong support.

Saeideh Shekari-Namin
Bergen June2012

Abstract

Small scale deformation structures that mostly occur in highly porous rocks are called deformation bands. Petrophysical characteristics of deformation bands are different from those of host rock and they can act as barriers or conduit to fluid flow. The effect on fluid flow is the most important property of these structures which is essential in many geological fields; for instance oil & gas, CO2 storage and ground water flow, when permeability and capillary pressure are the two major characteristics of the reservoir under study.

In this study, fluid flow experiments have been conducted on deformed sandstone sample from Moab member of Entrada Formation in Waterfall Canyon, Utah which contains cataclastic deformation bands. We have visualized one- and two-phase fluid flow in the deformed sandstone. According to Gamma-Ray scanning, the bands in this sample are denser than host rock and porosity and permeability in these bands were expected to be lower than the surrounding un-deformed rocks.

In miscible displacement experiment, five brine floods through sandstone with deformation bands was monitored using real time X-Ray image scanning instrument. To visualize the flow of fluids through the sample, injection water was saturated by Natrium Iodine (NaI) tracer. Removal of NaI tracer was done by injecting water saturated with NaCl with the same density of NaI. In two phase experiment, first a full saturation of sample with NaI as water phase was performed and thereafter draining of that was done using n-Decane ($C_{10}H_{22}$) as oil phase. Saturation in sample for water phase and oil phase has been estimated as 55% and 45%, respectively. Five experiments were performed with different inlet and outlet settings. The flow pattern showed a complex, but repeatable trace of fluids through the sample as fluids crossed deformation bands at same place in all experiments. In the two phase experiment the oil did not completely replace the brine which might be due to increased capillary pressure in the deformation bands.

Thin section study was performed on the same sample after the experiments to estimate porosity and permeability from Back scatter Electron Image analysis (BSE) of the deformation bands as well as the host sandstone. Estimated permeability for deformation bands are between 350mD and 900 mD and for host rock is between 1500mD and 2000 mD. Flow experiments and porosity and permeability estimated from BSE are in agreement with each other and the former works (e. g. Torabi et al, in press, Torabi & Fossen 2009 and Antonellini & Aydin, 1994) showing lower porosity and permeability in deformation bands comparing to host rock. Furthermore, this work gains insight into the actual flow of fluids through deformed sandstones by visualizing the flow pattern.

Table of Contents

Nomenclature

c	constant related to pore-geometry
F	Formation factor
f	(i,j)Characteristics or indicator function equal to 1 or 0 based on pixel positions
ϕ	Porosity
i, j	pixel positions in 2D BSE images
k	Permeability
m	Archie's cementation factor
s	Specific surface area of tubes
S_1	One point correlation function
S_2	Two point correlation function
Sn	(x,y) n = 1, 2,. . . N-point correlation function for distance in Cartesian coordinates

LIST OF FIGURES

LIST OF TABLES

1 Introduction

1.1 Background

Small scale deformation structures, so called deformation bands mostly occur in highly porous rock and sediments (Aydin 1978). They form as a result of strain localization and accumulated compaction or dilation or shear. They commonly form during the initial stage of the faulting process but also can form and grow in the damage zone of an existing fault (Rykkelid & Fossen, 2002, Torabi & Fossen, 2009). Deformation bands are formed throughout many reservoirs as it is observed in the North Sea (Gabrielsen & Koestler 1987). These structures are important reservoir heterogeneities in faulted reservoirs; because petrophysical characteristics of deformation bands are different from those of host rock and they can act as barriers or conduit to fluid flow. Their effect on fluid flow is the most important property of these structures which is essential in many geological fields; for instance oil & gas, CO2 storage and ground water flow, when permeability and capillary pressure are the two major characteristics of the reservoir under study.

Properties influencing fluid flow in deformation bands are mainly dependent on the rock composition and deformation mechanism. These properties vary in different dimensions of the bands, introducing more heterogeneities and anisotropies to the reservoirs. It is important to understand the details of the mechanical and physical structure of the bands in order to predict their behaviour in reservoir sandstone, where the interaction between the bands and fluid flow plays an important role in the production and/or storage of the reservoirs.

The role deformation bands exert on reservoir performance has been given lots of attention lately (e. g., Aydin 1978, Fossen & Hesthammer 1998, Torabi & Berg 2011) . Studies have been carried out mostly on physical characteristics and cataloguing type of bands (e.g. Fossen et al, 2007). There are several analyses on deformation bands' permeability and porosity; mostly using traditional permeability measurements using an inch-size plug for laboratory testing and mini permeameter in the field which are usually associated with uncertainties and difficulties related to both sampling and measurements. Also, image processing methods has been used (Torabi & Fossen, 2009) for permeability estimation and quantifying the spatial variation of grain size, porosity, and permeability within deformation bands through a

microstructural study. Some studies in petrophysical properties of deformation bands digs more and observe capillary pressure, irreducible water saturations (Ogilvie & Glover 2001), relative permeability, and moisture content (Sigda & Wilson, 2003 and Torabi et al. in press).

1.2 Aim and motivation of study

Most of the studies (e.g. Antonellini & Aydin, 1994 and Gibson, 1998) performed on fluid characteristics of deformation bands have been mainly concentrated on estimation of porosity, permeability and capillary pressure. Therefore, we noted that a practical experiment for visualization of fluid flow through deformation bands, beside the investigation about the related petrophysical parameters will be very useful to simulate their behaviour in reality. Flow mapping is also important to find out if decreased porosity, permeability and pore sizes are capable of trapping oil in the upstream host rock due to severe loss of relative permeability to oil in the deformation band. Even though, there are several studies about petrophysical characteristics of deformation bands, still there is a demand for more research; specially, to investigate more about fluid flow and its pattern in deformed sandstone reservoirs.

In this study, we conducted fluid flow experiments on deformed sandstone sample that includes deformation bands. We aimed to visualize one- and two-phase fluid flow in the deformed sandstone. Fluid pattern through single intersected bands and cluster of bands are illustrated. We also performed thin section study on the sample after the experiments to estimate the petrophysical properties of deformation bands as well as those of the host rock in order to correlate the results of thin section study with the experimental results. The variation of petrophysical properties of bands have been captured by image processing of BSE images of thin sections and have been compared with the results of fluid flow experiments.

2 Deformed porous sandstone and its petrophysical properties

2.1 Fault zone structures

2.1.1 Fault zone architecture

A fault is generally a zone of deformed rocks instead of being a plain surface. Fault zone architecture is usually complex and has wide range of variety. This variety has base in lithology, burial depth, stress conditions and displacement (Berg et al., 2004). Fault zones are generally described by distinct components, such as a fault core, damage zone and an un-deformed protolith (Fig 2-1) - The fault core refers to the central part of the fault which is defined as the volume of the fault that has gained the most of bulk displacement. Fault cores consist of the crushed or smeared rock, slip surfaces, and diagentiacal altered rocks. . This zone consists of bulk portion of strain and displacement and includes the variety of different structural elements (Berg et al., 2004).

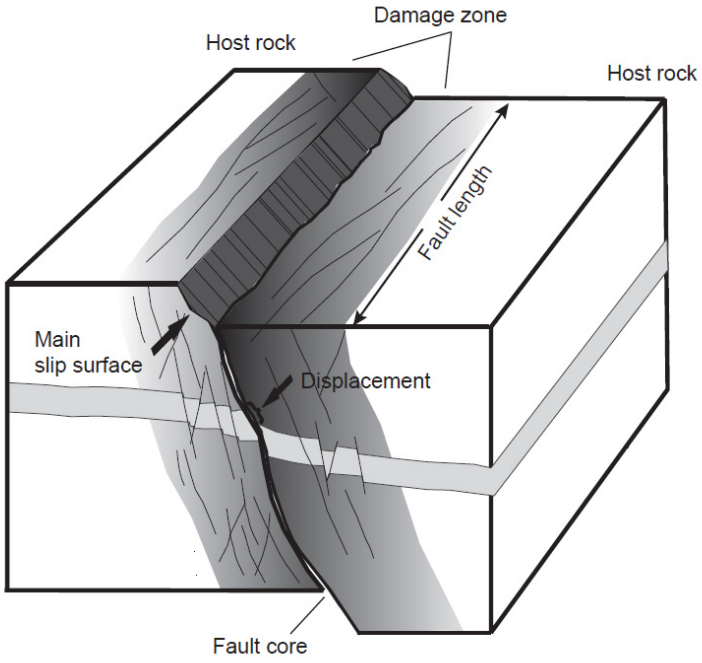

Figure 2-1: Schematic illustration of fault core and damage zone in siliciclastic rocks (Kolyukhin & Torabi, 2012).

The damage zone that surrounds the fault core consists of deformational structures like shear fractures, veins (joint filled with cement) and deformation bands. The density of fractures and

deformation structures commonly increases toward the main fault (e.g. Berg et al. 2004). The damage zone width and fault core thickness show a positive correlation with the displacement of the fault (Torabi and Berg, 2011 and the references therein).

Deformation pattern in damage zones of faults in porous rocks is often associated with strain hardening of rock resulting in formation of deformation bands. The evolution of a major fault in sandstone may be ascribed to a formation of a wide deformation zone in front of a propagating tip line, described as the process zone (e.g. Shipton and Cowie, 2003) .Structures in damage zones are thus the results of both structures formed in process zone and during slip of fault.

2.1.2 Deformation bands in fault zone

Deformation band are commonly present in clastic reservoirs and aquifers and may form in many tectonic settings including, extensional, compressional, strike slip, as well as glacially, gravitationally and salt diapiric deformed sands and sandstone sediments (Figure 2-2).

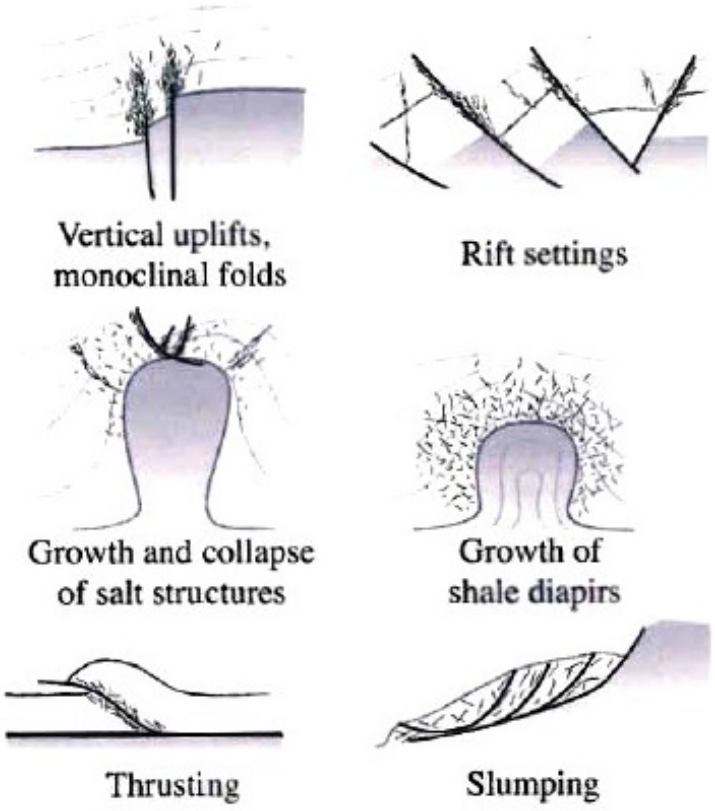

Figure 2-2: Different setting where deformation bands commonly develop (Fossen et al 2007).

Deformation band is one of the primary elements in the process of growth of fault zones in porous sandstone (Antonellini & Aydin 1994).They have been widely observed as cluster around damage zone and process zone of large faults. Deformation bands also occur as isolated (individual) structure, linked system, complex zone of multiple interconnected deformation bands in fault zones (Figure 2-3). Displacement increases respectively from mm to few tens centimetres for mentioned types.

First stage of fault growth in porous sandstone is formation of single deformation band. Deformation bands form by collapse of pore space and cataclasis which cause increase in cohesion and strengthening of the band compared to the surrounding sandstone. Further strain hardening process will continue to the formation of another band in the vicinity of the existing band (Fossen et al, 2007). Creation of more bands will lead to creation of links between bands and clusters are formed. Continuous formation of deformation bands and linkage between them eventually results in developing the fault slip surface (Fossen et al, 2007).

In fault zones, single deformation bands can usually be located far (hundreds of meters) from slip surface of fault. Approaching the fault surface, the density of deformation bands increases and clusters of deformation bands are present. The, complexity and interconnectivity increases often seen as anastomosing pattern of deformation bands close to fault surface.

Deformation bands should not be mistaken with faults, slip surface or tension fractures. Main difference between deformation bands and ordinary faults is that deformation bands do not have continuous slip surface. The displacement of deformation band are in micro scale order and not much longer than the maximum grain size (Fossen & Heshammer 1998). Another difference between ordinary fractures and deformation bands is that cohesion is maintained or increased in most deformation bands, where as it is reduced for slip fractures and tension fractures.

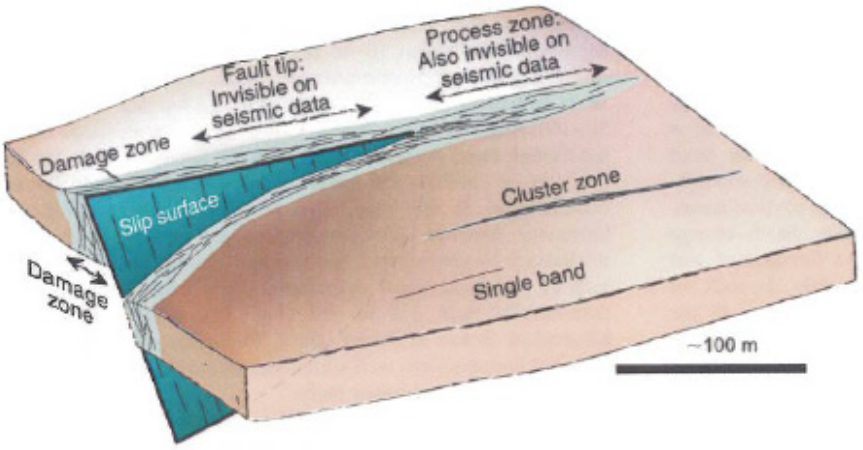

Figure 2-3: Fault tip in porous sandstone. Deformation bands are formed in the 'process zone' ahead of the fault tip (Fossen et al, 2007).

2.2 Classification of deformation bands

Deformation bands can be classified both kinematically and based on dominant deformation mechanism operating during their development.

2.2.1 Kinematic classification

Based on previous studies (e.g. Aydin et al.2006) kinematic classification can be presented as dilation bands (pore volume increase), shear bands (no pore volume change), compaction bands (pore volume decrease) or combination of these types (see Figure 2-4). Most of deformation bands are compactional shear bands formed by compaction and grain crushing. Compactional and shear band are most common where dilation bands are rarely observed (Fossen et al., 2007). However, some evidence shows that deformation bands were dilatant and permeable at an early stage of band development (Parry et al., 2004).

2.2.2 Mechanism based classification

Deformation mechanism is depended mainly on stress, grain size, shape, mineralogy, porosity and cementation. The main deformation mechanisms are (Figure 2-5):

- Granular flow: rotation and boundary sliding of grain
- Catalasis: flaking and splitting of grain
- Phyllosilicate smearing
- Dissolution and cementation

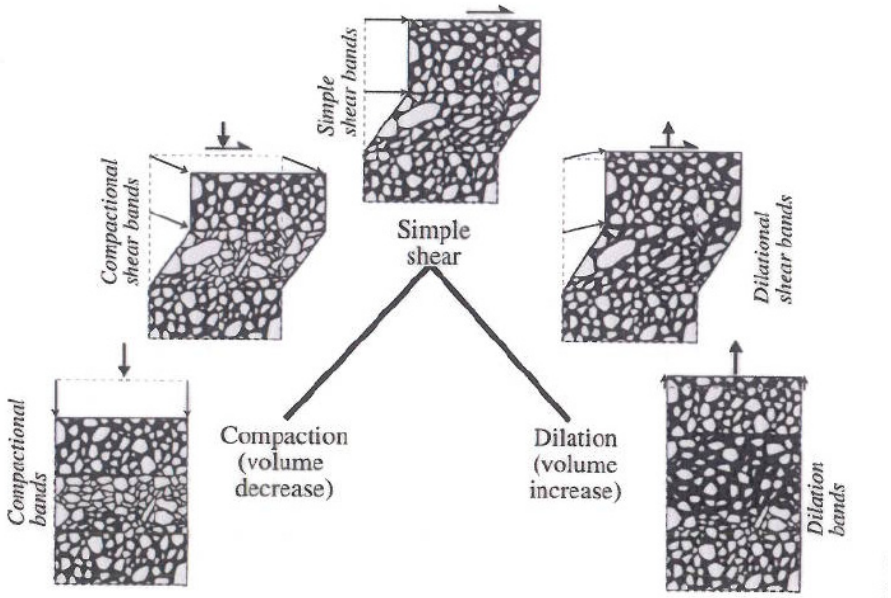

Figure 2-4: Kinematic classification of deformation bands (Fossen et al. 2007).

Deformation mechanism is related to the condition for formation of the band and the initial petrophysical properties of the host rock. This classification includes: disaggregation bands, cataclastic bands, phyllosilicate bands, dissolution and cementation bands.

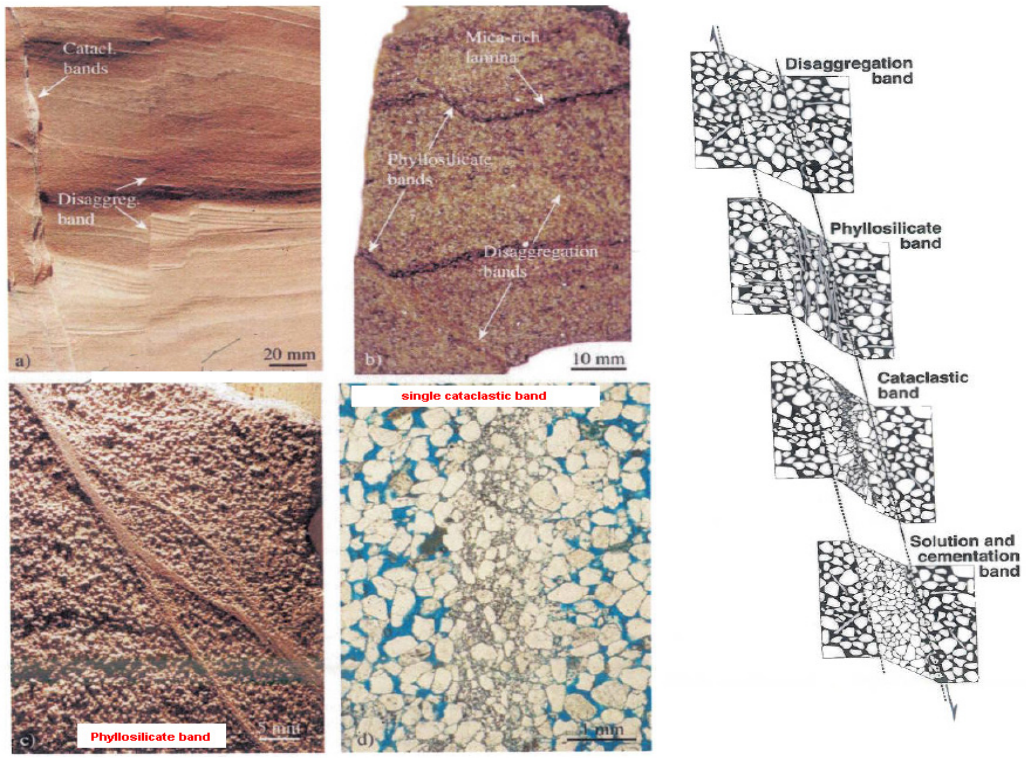

Figure 2-5: Classsification of deformation bands based on mechanism of deformation (Fossen et al, 2007).

Importance of deformation band characteristics and their effect on fluid flow needs understanding of the the condition and factors that influence formation of deformation bands. Important factors can be addressed as confining pressure, tectonic environment, pore fluid pressure and host rock properties like mineralogy, grain size and grain shape. Some factors are subjected to change in different burial depth and some (e. g. permeability, porosity and cementation) change during the time. A temporal sequence of deformation band therefore has been defined (Fossen et al., 2007) related to depth and phyllosilicate content (Figure 2-6). In sandstone, usually the earliest type of deformation band is formed as disaggregation band related to low confining pressure often in local non-tectonic gravity controlled deformation (e. g. local shale diapirism, underlying salt movement and gravitational sliding). Cataclastic bands that form in shallower depth in poorly consolidated sands show less intensity of grain crushing than those formed at higher depth. Phyllosilicate bands can form in different depth where the content of phyllosilicate is around 15%. Lithology also plays important role in controlling of formation of deformation bands. Well-sorted sandstone, higher porosity and larger grain size improve condition of formation of cataclastic bands. Similarly, higher phyllosilicate content, lower porosity and smaller grain size leads to the formation of phyllosilicate bands (e. g. Johansen et al, 2005).

With deeper burial depth porosity is commonly reduced due to lithification formed by compaction and diagenesis (quartz or clay cementation). In these settings a possibility of deforming the rock by crack propagation is more likely than collapse of pore space and slip surfaces, joints and veins can be developed. . Observed in fault zones, the temporal sequence of deformation in porous sandstone may be as respectively; deformation bands, faulted deformation bands (slip surface), joints and reactivated joints (faults) in porous sandstone (e. g. Johansen et al, 2005).

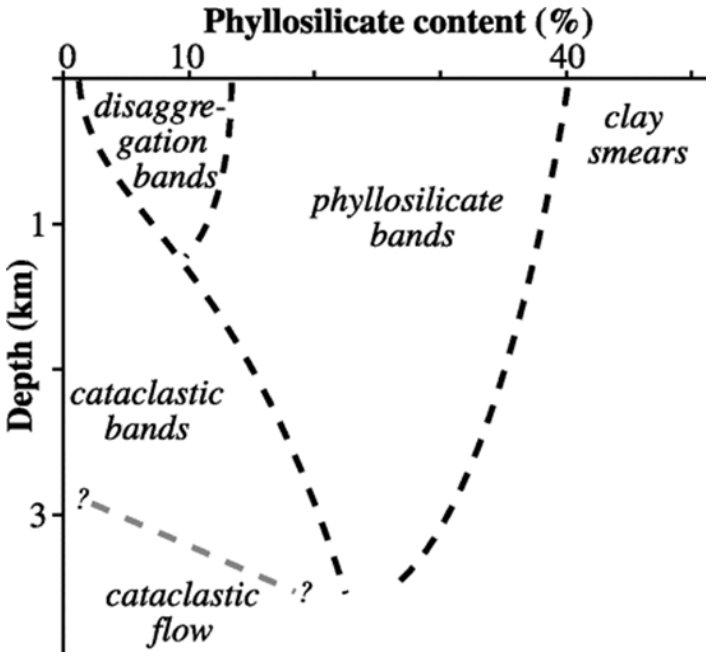

Figure 2-6: Illustration of variety of deformation bands related to different depth and phyllosilicate content (Fossen et al, 2007).

2.3 Specifications of different types of deformation bands

2.3.1 Disaggregation bands

The mechanisms involved in these types of bands are grain rolling, grain boundary sliding and breaking of grain bounding cements and they form in shallow burial depth. These processes are typically called granular flow or particulate flow. These bands usually have length about a few 10 meters and thickness around 1 to 5 mm depending on the grain size and they may be difficult to recognize in homogeneous quartz sandstones. They mostly involve little change in petrophysical properties of sandstone (Fossen et al, 2007).

2.3.2 Phyllosilicate bands

If the phyllosilicate content of the host rock is higher than ~15%, phylosilicate band is likely to form. Also, when the phyllosilicate or content of host rock is high (more than 40%) a clay smear surface will be developed (Fisher & Knipe, 2001).

2.3.3 Cataclastic bands

The main mechanism involved in these bands is grain fracturing. As it is shown in Figure 2-5_a&d they are usually visible and the core of bands holds wide range of grain size, where in the surrounding region moderate grain fracture and compaction view is recognizable. Cataclastic band is a common type of deformation bands; hence they have been the focus of many research studies (Fossen et al, 2007).

2.3.4 Dissolution and cementation bands

Dissolution and cementation can occur in deformation bands during or after (mostly) deformation. Dissolution is a typical feature of deformation bands formed in shallow burial depth. If dissolution (known as chemical compaction or pressure dissolution) dominates, the band is called dissolution band. Dissolution bands show little or no fractures and they include lightly packed grains (mostly quartz). Cementation bands occur during grain crushing or boundary sliding where the fresh and highly reactive surfaces acts as promoting elements. Cementation occurs specifically where there is coating of undeformed host rock by diagenetic

minerals. In deformation band this coating is broken by sliding and fracturing (Leveille et al. 1997) and therefore promotes cementation within the band.

2.4 Petrophysical properties of deformation bands

As it was mentioned previously, the significance of the study of deformation bands is in their behaviour versus fluid flow which is important for predicting fluid flow in sandstone reservoirs or in any other relevant field (e.g. CO_2 storage underground and underground water). Therefore, there has been a focus in recent studies (e.g. Torabi & Fossen, 2009) on the properties of the bands which have the main effects on fluid flow (e. g. Porosity and Permeability). These petrophysical properties will be discussed in following paragraphs for different types of deformation bands as classified before.

2.4.1 Porosity and Permeability

Most previous studies show that deformation bands reduce permeability of sandstones (Fossen et al., 2007). However, some cases (e. g. Sample et al., 2006) show higher permeability leading to increased transmissibility in reservoir. Figure 2-7 shows two different type (dilation (to the left) and compaction (to the right)) of deformation band in the same layer which show different behaviour (conduit and barrier) regarding to fluid flow.

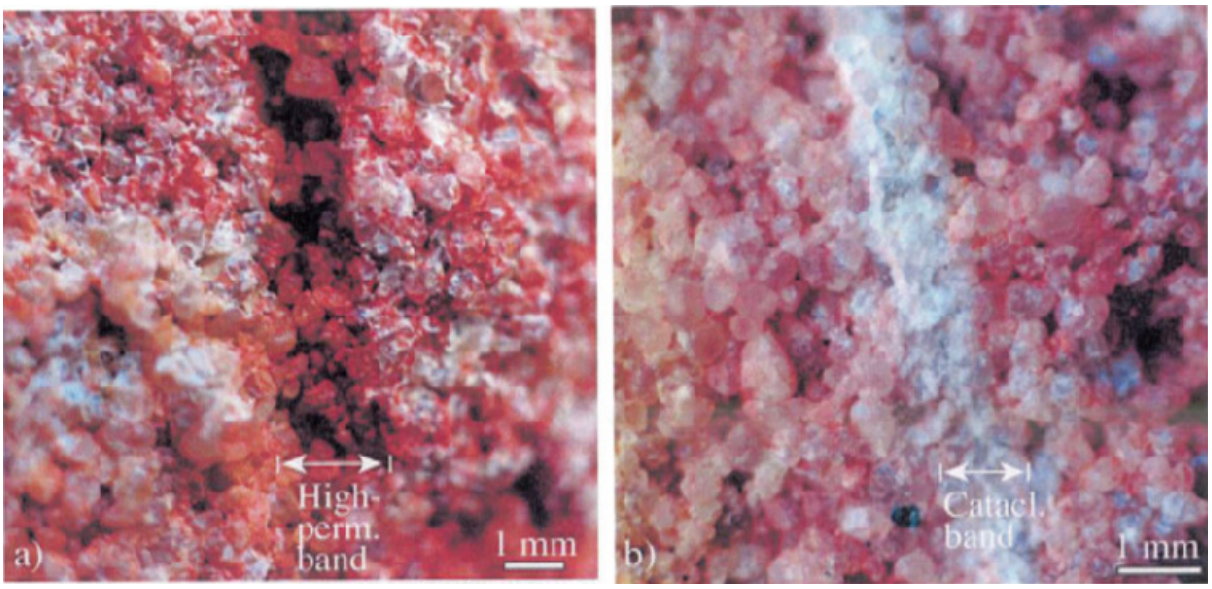

Figure 2-7: Two deformation bands in the same layer of Nubian Sandstone (Fossen et al, 2007). a) Disaggregation band with higher porosity than host rock. b) Cataclastic band with highly reduced porosity.

Microstructure, porosity and permeability vary widely along the deformation bands (even in a single band). Torabi & Fossen (2009) have estimated the variation in porosity up to 18% and permeability up to two orders of magnitude. This variation in different developing mechanism depends on the degree of cataclasis, dissolution or phyllosilicate content. These variation plus continuity, direction and the placement of deformation bands in cluster / zone are important in studying fluid flow in reservoir with deformation bands, where their position and intersection in cluster /zone impact the ability of bands acting as barrier in reservoirs.

Disaggregation bands:

Both increase and decrease in porosity is possible to occur in these bands depending on their component whether it is a dilational band or a compactional band. Increase in porosity and permeability in disaggregation bands is transient and pore space usually is filled later by clay-rich cement resulting in decrease of porosity and permeability (Du Bernard et al, 2002). In general, changes in porosity and permeability in these bands are relatively low compared to other types of bands and their reported permeability reduction is up to one order of magnitude (Fisher & Knipe 2001).

Phyllosilicate bands:

Phyllosilicate bands reduce permeability, because of mixing and alignment of platy minerals and shear strain. This reduction is depended on the quantity of phyllosilicates, their type and their distribution and for North Sea reservoirs, their reported permeability reduction is around two orders of magnitude but could locally be more (up to 5 orders, Fisher & Knipe, 2001).

Cataclastic bands:

In general, porosity in these bands is one order of magnitude smaller than the related host rock which causes the reduction of permeability up to three orders of magnitude (Torabi & Fossen, 2009). Measurements (e. g. Antonellini & Aydin, 1994) on some core of well-developed cataclastic shear bands with very low porosity (less than 1%) shows permeability as low as 0.001 mD. Permeability reduction in experimentally produced cataclastic compaction bands is reported by Holcomb & Olsson (2003) as two orders of magnitude.

Dissolution and cementation bands:

Mechanical crushing and reorganization of grains during cataclasis and dissolution promotes the condition for cementation. Cementation process start during formation of deformation

bands but it may mostly take place after (Fisher & Knipe, 2001). With increasing burial depth, dissolutions and precipitation of quartz becomes faster and that may be the reason for observation of general decrease of permeability with depth in cataclastic bands of southern North Sea (e. g. Fisher & Knipe, 2001). The transient increase of permeability combined with initial dilation ease entering of reducing fluid to the band and results in lightening of colour and this mechanism may explain cementation in low porosity cataclastic deformation bands (e.g. Bernabe & Brace 1990).

2.4.2 Capillary pressure

Faults and their associated deformation bands are tabular zones whose sealing capacity is controlled by their intrinsic properties (Fisher and Knipe, 2001). The capillary seal of faults is assessed where the sealing capacity of the fault zone relies on the size of pore throats and capillary forces between wetting and non-wetting phases (Torabi et al., accepted). The capillary seal model allows for partly sealing faults, where the sealing capacity is governed by a critical pressure difference across the fault, i.e. an equilibrium situation acquired over geologic time in petroleum reservoirs that may be altered during production or injection (Fisher et al., 2001; Jolley et al., 2007, Torabi et al., in press). When the critical pressure is overcome for the liquid/vapor in question, flow is controlled by the relative permeability of flowing mediums (e.g., Manzzochi et al. 2010).

Most of the deformation bands increase capillary pressure of reservoirs and results in trapping of hydrocarbon column (the highest calculated is up to 80 meters for a cluster of cataclastic bands, (Torabi et al., in press). Low permeability deformation bands (e.g. low porosity sandstone) can influence the movement of fluid in producing reservoirs by increasing capillary pressure in the reservoir.

3 Sample description

The sample used for our study has been taken from Moab member (quartz arenite) of Entrada Formation (Middle Jurassic) in Waterfall Canyon, Utah (Figure 3-3). The sample comes from damage zone in the footwall of Moab Fault with bulk dimension of 122x49x12 mm^3 (average thickness) and contains cataclastic deformation bands (as shown in Figure 3-1 and 3-2).

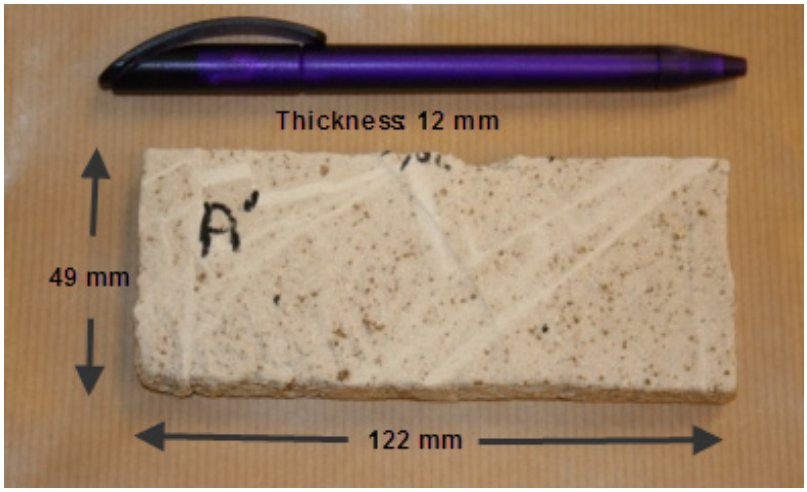

Figure 3-1: Front photo of sample A'.

Figure 3-2: Flip side of sample A'.

The footwall in Waterfall Canyon is dominated by deformation bands running sub-parallel to the main fault direction. A number of deformation band frequencies in the footwall display a significant decrease in deformation band frequencies moving away from the fault core (Ellingsen, 2011). Stratigraphically, this is resting directly on top of the Slick Rock Member of Entrada Sandstone Formation. Host rocks of the Moab Member consist of light-yellow to grey coloured, fine to medium grained sandstone.

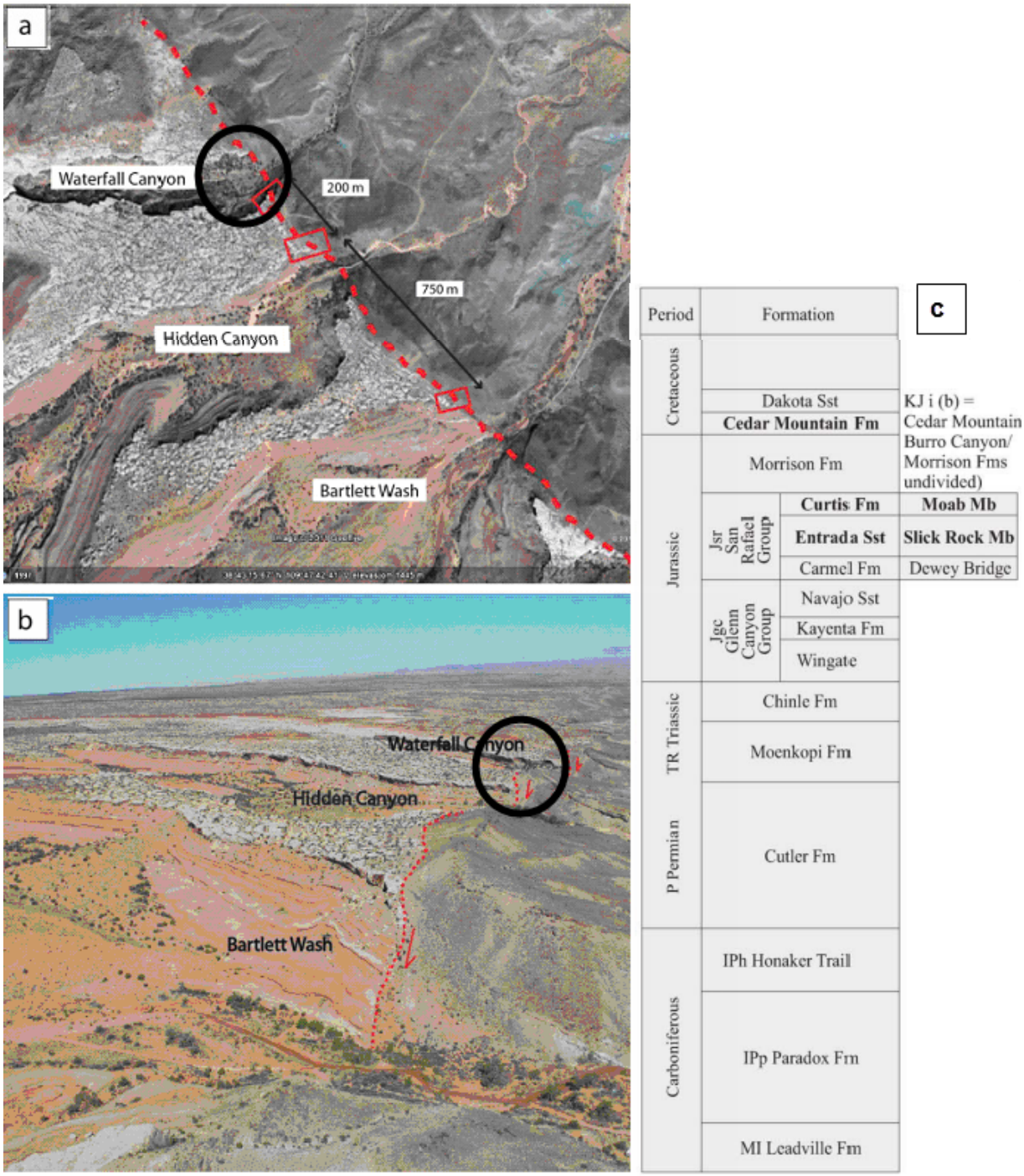

Figure 3-3 : Air image (a) and photograph (b) of localities in Moab Fault; location of Waterfall Canyon where the sample is taken. (Ellingsen, 2011), (c) stratigraphic column for the study area (Berg & Skar, 2005)

These mature, well sorted and well-rounded sands are typical sediments of aeolian desert environments and were deposited in widespread sand dunes in the Middle Jurassic, dunes that covered large areas of what is now the Colorado Plateau. The thickness of this unit is approximately 30 metres (Berg and Skar, 2005). The more homogeneous and continuous

nature of the footwall rocks made it possible to follow an entire layer for the entire permeability profile. The measurements were collected perpendicular to bedding and parallel to the main fault by Ellingsen (2011). He reports that the general trend line is negative with permeability decreasing away from the fault core (Figure 3-4).

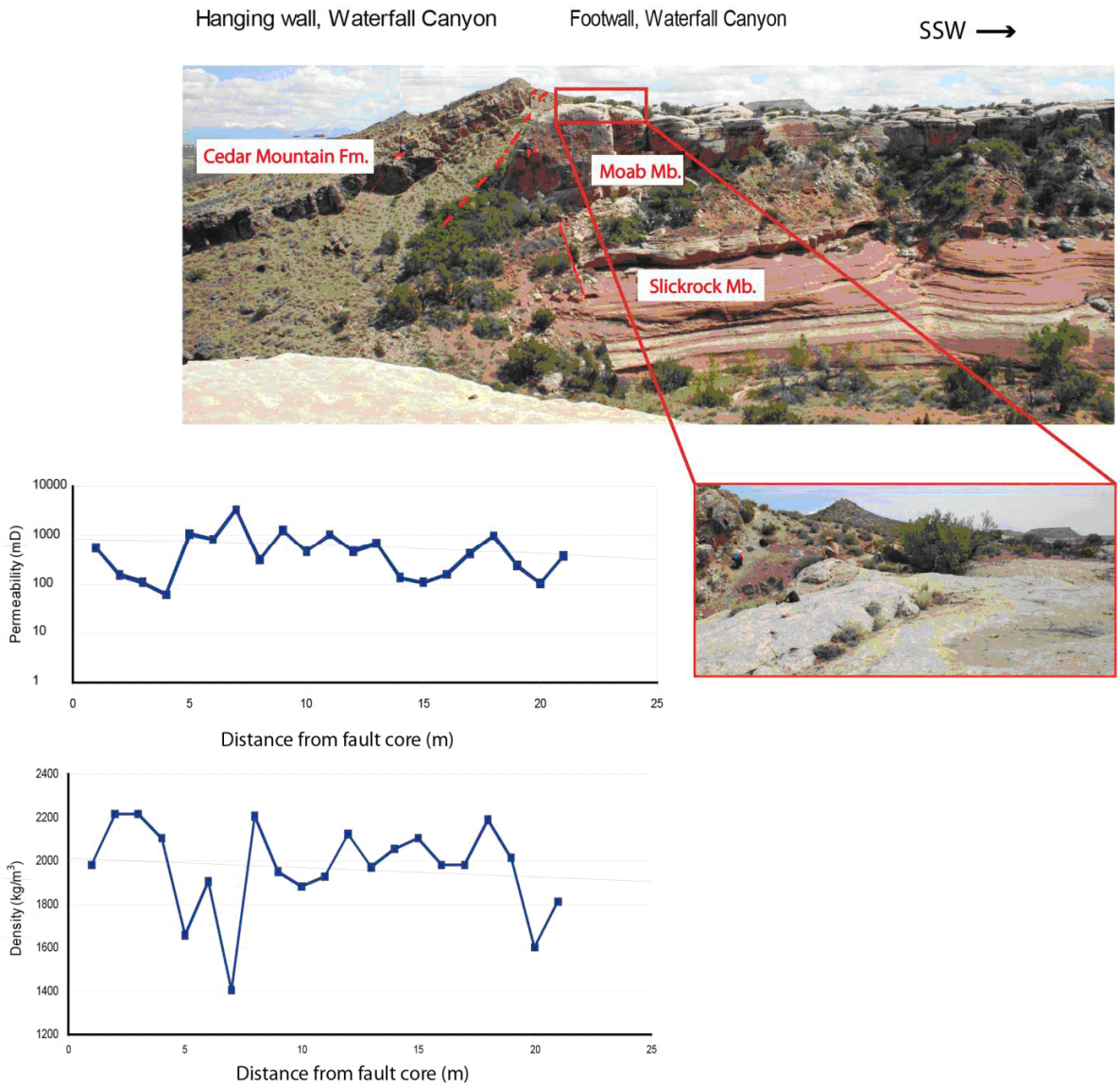

Figure 3-4: Permeability and density measurement from Moab Mb and their variation along distance from fault core (Ellingsen, 2011). Density measurements come from Schmidt Hammer Test.

4 Methodology

4.1 Fluid Flow Experiment

4.1.1 Instruments

X/Gamma-Ray scanner

The experiment has been performed at CIPR laboratory using a 2D X-Ray scanner. The scanner works based on quantitative attenuation. The rig is designed for both horizontal and vertical flow measurements, thus, both vertical and horizontal fluid flow can be examined (Figure 4-1). The rig has capacity for sample with the dimensions up to 1 x 1 meter.

Two types of measurements can be provided by the scanner:

1) Real time X-Ray imaging by X-Ray camera

2) Photon counting of X-Ray and Gamma-Ray attenuation.

Figure 4-1: 2D Core Scanner shown in horizontal and vertical position.

The scanner cabinet is placed on a steel frame with two doors that can slide and make inside scanner accessible and an inspection window for checking the sample and system from outside. Cabinet has also a safety sensor which makes sure that doors are closed before scanning.

Instead of one sample up to 1x1 meter size, several smaller samples can also be positioned in the cabinet at the same time letting simultaneous flow measurements on different slab samples (Figure 4-2). Scanning parameters for both image scanning and photon counting are

controlled by two independent software programmes, also able to calibrate for different configuration.

Figure 4-2: Four slabs mounted in the scanner cabinet. (Noremark, 2010).

Scanning area is divided into a 9 x 9 matrix of smaller areas, allowing for individual scanning of 81 different areas. Dimension of each area is 11 x 11cm and the areas to be scanned are selected on the computer software.

X-Ray imaging

Real time X-Ray imaging uses an image intensifier (X-Ray camera) which suites for illustration of flow patterns and flow compositions within the sample. The X-Ray camera allows for rapid snap shots of dynamic flow processes.

An ultra-sensitive linear array detector moves across the sample while X-Ray source moves simultaneously on the other side, creating an attenuation image. Each image is constructed of thin image strips which are 6.4mm in width and 120mm in height. They are assembled and memorized as JPG pictures by the computer software. Pixel resolution is 0.001cm and the angle of X-Ray emission used for image scan is typically 20°. The JPG picture is an array of integers from 0 – 256 (256 shades of grey).

Absorption of radiation depends on the density/porosity of material (sample) and fluid saturation. Different detected intensities are printed with varying grey levels (darker for

denser areas). To identify multiphase fluids in sample usually brine is doped denser (darker) rather than oil. Therefore, existence of oil in sample's porous area makes darker contrast than dry sample and existence of brine improves the contrast. Figure 4-3 illustrates Schematic of X-Ray imaging system in the rig.

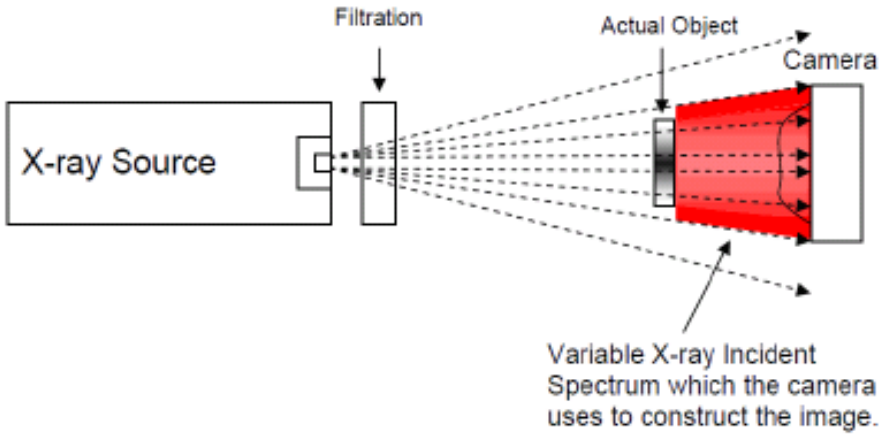

Figure 4-3: Schematic of X-Ray imaging system in the rig (Horgen, 2010).

The intensities being detected by the camera can be in the range of 0 – 65000. These are called threshold values, and low values are printed as very dark/black whereas high values are printed as very bright/white. According to porous medium being scanned, different threshold values can be used. When narrowing down the threshold range, all intensities that are not within this range are printed as just black or just white. By doing this, a more focused or sharp image is produced. In these experiments the samples were scanned with threshold values 0 – 7500. The X-Ray unit can be operated between 40 and 60 kV at a maximum current of 0.4 mA. This means that the maximal energy of X-Rays emitted from the X-Ray tube is 60 kV, and the maximal current of electrons in the tube is 0.4 mA. The energy ranges used in the experiments are 60kV with current 320μA.

X/Gamma-Ray photon counting

Radiation source can emit low energetic narrow beam of both X-Ray and Gamma-Ray. A scintillation detector for photon counting of X/Gamma-Ray attenuation provides an accurate assessment of the actual composition of the sample and the flow constituents across. The detector measures the intensity for each step. The data is saved uncompressed in text format. The maximum intensity the scintillation detector can measure is approximately 30,000 counts per second, but detection rate is recommended to keep below 22.000 counts per second, in

order to stay below a count error of 2%. In the rig there is a collimator in front of the photon detector. A collimator is a device that is used to filter a stream of rays so that only those travelling parallel to a specified direction are allowed through (Figure 4-4).

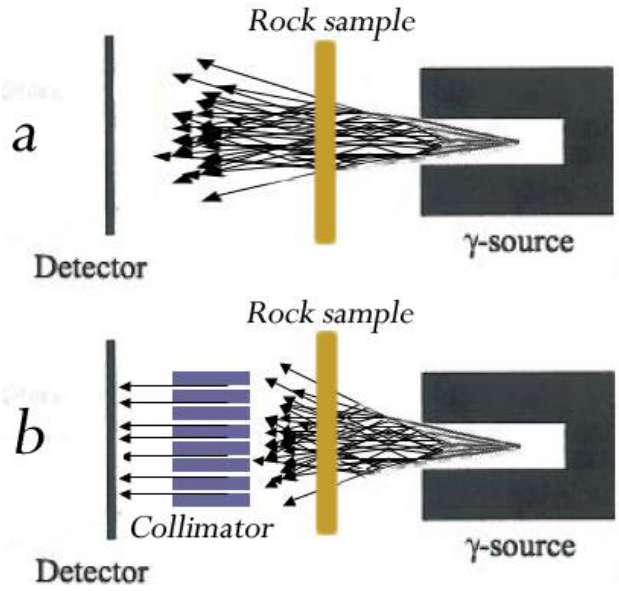

Figure 4-4: Photon counter detector without collimator (a) and with collimator (b).

4.1.2 Sample preparation and setup

Epoxy-coating

During the fluid flow experiment, fluid should be confined in the sandstone and this is done by coating the sample with epoxy. The epoxy used for this purpose is made from 20% resin GC 15 and 80% Axon GC1 150. Three layers of epoxy coating were put on the sample carried out in several steps. Two nails are used as mark to ease further adjustment of position of sample in photos. A metal attachment with some holes helps to have better mounting of the sample in the rig. Figures 4-5 and 4-7 show the sample under and after epoxy coating.

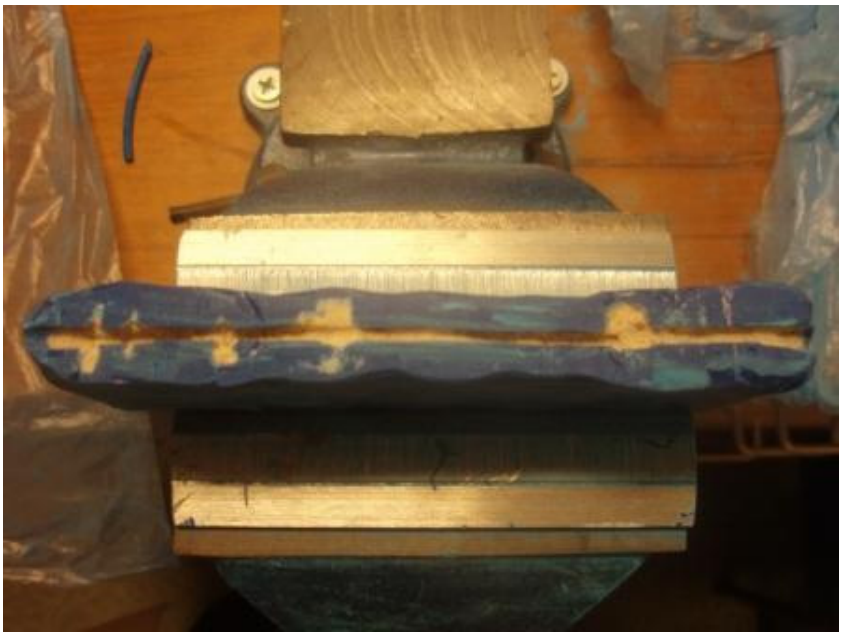

Figure 4-5: Sample A´, under preparation (epoxy coating).

Inlet/outlet

Four inlets are placed around sample A´ based on the position of deformation bands in a way that gives us the best possibility of studying fluid flow across the deformation bands; two inlets are put in the drilled holes located in the middle of upper long edge and perpendicular to that. The other pair is placed at end of the groove made along the lower longer edge and parallel to that (connecting tube laid in groove and covered by fibre paper and epoxy which will conduct the fluid flow in the sample). Position and numbering of inlets/outlets and the attached metals are shown in Figure 4-6:

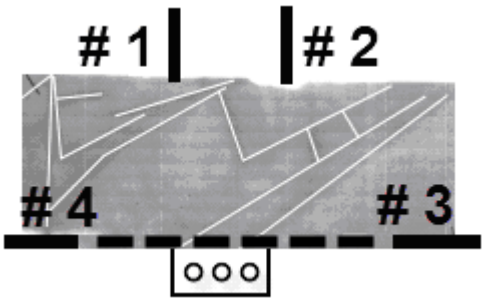

Figure 4-6: Position and numbering of inlets/outlets.

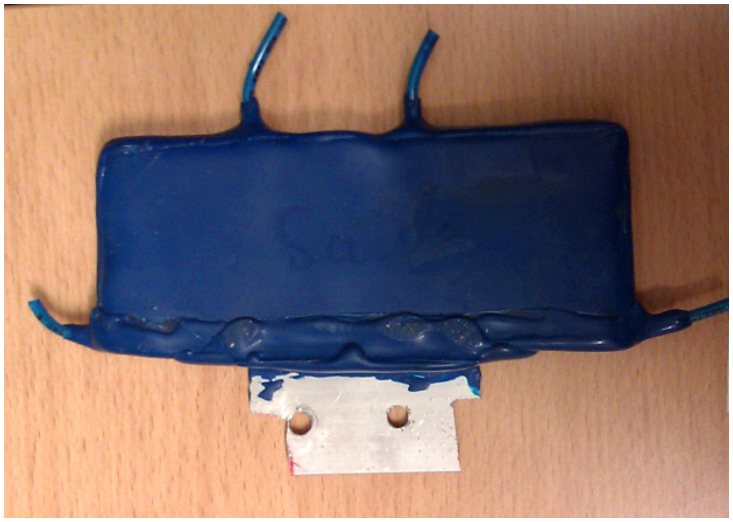

Figure 4-7: Sample after epoxy, ready to be scanned in rig.

Leakage (vacuum) test

Encapsulated sample in epoxy coating should be tested for any possible leakage. For this purpose, sample was hold under vacuum condition applied by a pump connected to valve 4, while valves 1 and 3 were kept closed and valve 2 was connected to a cylinder (Figure 4-8). Coated sample shows good sealing where the pressure read from the gauge connected to valve 2 was dropped from 770 mbar to 2 mbar in about 2 hours.

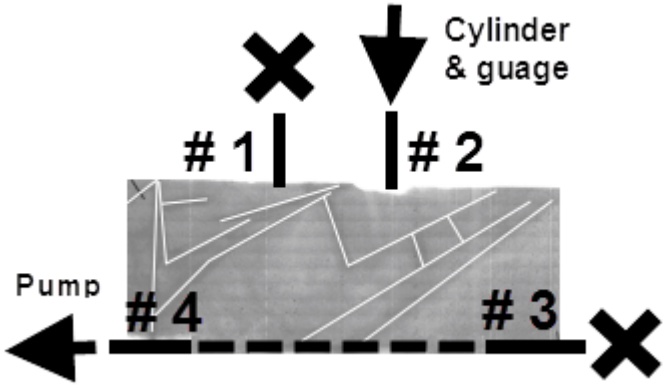

Figure 4-8: Configuration for leakage test.

4.1.3 Gamma measurement (Saturation test)

The purpose of this test was to visualize the fluid (NaCl) distribution and its saturation in the pore system of the sample. Am-241 Gamma-Ray scan and photon counting technique were used in this measurement.

Counting of photons is performed by measuring of attenuation in a scintillation detector. It gives good accuracy for composition of fluid, air and solid sample. Attenuation of fluid can be measured separately and compared with combined (saturated) attenuation for calculation of porosity. Photon beams are created by Gamma-Ray (or X-Ray) source and an aluminium filter is used to emit only direct narrow beam of radiation. Attenuation of beams passed the sample is measured by a sensor in other side and saved as a data in the computer connected to the scanning instrument. These data matrixes are assembled using proper codes in Matlab (presented in appendix B) in order to better visualize fluid distribution or calculate porosity and saturation.

First, a test scan was run to adjust the integration time, steps and range of scanning area. Then, two scans were run for dry and saturated sample with NaCl solvent. Configuration and result of this measurement is presented in Section 4.1. Configuration of inlets/outlets is the same as for Figure 4-9.

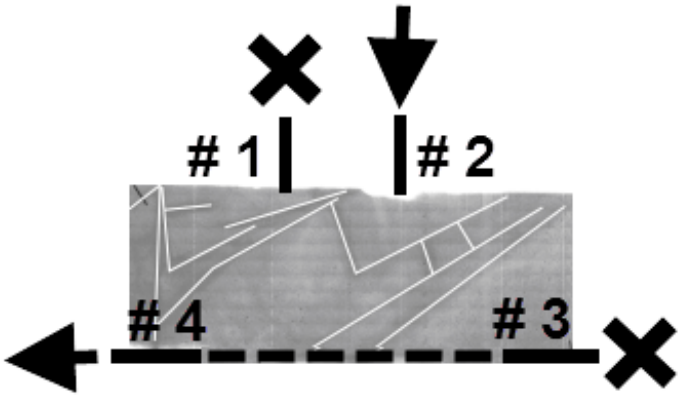

Figure 4-9: Gamma measurement configuration.

4.1.4 Porosity estimation

Because of uneven thickness of the sample gamma measurement was not used for porosity calculation. Therefore, porosity of sample is estimated based on conventional material balance approach. Porosity would be volume of pore space divided by bulk volume of sample. Volume of sample was estimated based on direct measurement as 71736 mm^3 (49x122x12). Volume of injected solvent is measured by test instrument which was 18065 mm^3. Then, the porosity could be estimated approximately 25% (18065 / 71736 = 0.252).

4.1.5 Miscible displacement

Main part of experiment was monitoring of miscible displacement through deformation bands using X-Ray image scanning program. For better contrast between fluids the brine was doped with NaI. The brine was made from solving of 100 (and 70) gram NaI in 1liter distilled water. Removing of doped brine was done by injecting NaCl with the same density of NaI. Injection has been carried out for different routes by opening or closing of installed valves.

4.1.6 Two phase flow (imbibition and drainage)

Imbibition:

In order to study the two phase flow in the sample NaI solvent with density of 100g/L is used as water phase and the sample is saturated in two steps from inlet 1 and 2 while valve 3 was outlet and respectively valve 2 & 4 and 1 & 4 were kept closed (Table 5-3). The rate of injection in both steps was 20 ml/h and duration was 120 min.

Drainage:

Thereafter, oil phase which is n-Decane ($C_{10}H_{22}$) in our experiment is started to be injected and drain the sample. This replacement is also been set in two steps as the same valve configuration mentioned for imbibition. The drainage procedure has been monitored by Real time X-Ray imaging (60 kV, 319 μA, threshold: 0 – 7000).

4.2 Thin Section Analysis and Image Processing

Traditional permeability measurements (inch-size plug and mini-permeameter) are not precise enough to measure permeability of single deformation band in porous sandstones which is few mm thick. Laboratory-based plug measurements represent the effective permeability across a 2.54-cm (1-inch) long sample, which includes a deformation band and its host rock. In this study we use the image processing method to estimate the porosity and permeability of deformation bands on the micro-scale using spatial correlation functions and a modified version of the Kozeny-Carman relation (Torabi et al., 2008). Using this method, we have no size limitation in the porosity and permeability estimations which typically is in traditional approaches.

4.2.1 Thin sections

In this project, we have studied 2 polished thin sections (MT1 & MT2 shown in Figure 4-10) of sample using optical and scanning electron microscopy. High-resolution photomicrographs from optical microscope have been used for estimating the porosity. Permeability of the selected locations (on deformation bands or host rock) of thin sections is estimated on backscattered electron (BSE) images of thin sections.

Figure 4-10: Location of thin sections on the sample.

4.2.2 Porosity estimation

To estimate porosity, high-resolution photomicrographs from optical microscope have been used for that cover the representative area of interest of deformation bands or host rock. The images have high resolution (1280x960 pixels) with the scale of 0.83 to 2.86 micro-millimetres per pixel. Formulation and procedure of MATLAB code used for porosity estimation (Torabi, 2008) can be described as bellow:

First an area of image (for instance 600x600 pixels) has been selected on the specific location which has the best representation for that specified location; locations are chosen to be on deformation bands, host rock and between deformation bands. It is possible to choose bigger or smaller area on image either square or non-square. But, further in next steps the non-square matrix should be converted to square one. We select parts of the image that has as less as possible broken grains at the edge of the image. Images are converted from coloured to grey scale ranged "0-256" because; in order to be able to use the indicator function to characterize the microgeometry of the samples the colour intensity range should be limited to two pixel values representing the two phases of the medium.

Next step is making binary images from grey scale using the estimated threshhold value by Otsu method. The intermediate pixels between white and black pixel values in the gray-scale images have proportions of black and white in their areas. When a threshold shade of gray is chosen, all pixels with gray above this threshold are white (grains) and all below are black (pores). Figure 4-11 illustrates a gray-scale BSE image (a) and related binary-reversed equivalent.

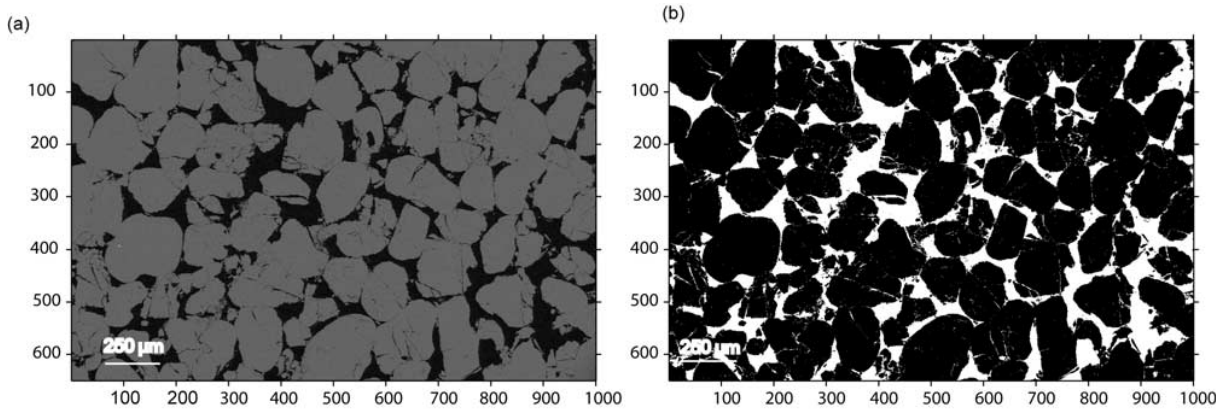

Figure 4-11: a gray-scale BSE image (a) and related binary-reversed equivalent (b), (Torabi et al, 2008).

The binary image has pixel value ‘‘0’’ in the pore space and ‘‘1’’ in the grain space. Since we are interested in void correlation functions, the binary image has been reversed to have ‘‘1’’ for voids and ‘‘0’’ for grains. Then we define a function f(i, j) that is zero for grains and one for voids, and (i, j) indicates the position of pixels in the image. Last step is to calculate the one point correlation function that is the porosity.

$$S_1 = \phi = [f_{(i,j)}] = \sum_{ij} f_{(i,j)} / (M \,.\, N)$$

i = 1,2,3,… M and j = 1,2,3,… N

4.2.3 Permeability estimation

In order to estimate permeability we use the same method used by Torabi et al [2008] that is a modified version of the Kozeny-Carman relation developed by Paterson [1983] and Walsh and Brace [1984]. For the process of permeability calculation, higher magnification (from 122X to 630X) and resolution (1024X768) BSE images have been used. The choice of magnification for the images depends on the grain size; hence, the area of the used images varies from sample to sample. The pores in porous media are considered to be tabular and then permeability can be formulated as:

$$k = \phi^2 / cFs^2$$

Where phi is the porosity, c is a constant related to pore-geometry that is equal to 2 for materials possessing pores of circular cross-section, and F is the formation factor and has an exponential relationship with porosity [Archie, 1942]:

$$F = \phi^{-m}$$

Exponent “m” is a cementation factor and it varies between 1.5 for poorly consolidated sandstones and 2 for well consolidated sandstones [Brace, 1977; Sen et al., 1981; Wong et al., 1984; Blair et al., 1996]. “m” is decided to be 1.8 for deformation bands.

"s" is the specific surface area of the tubes. The specific surface area (s, i.e., the total area of the pores divided by the total volume of the porous media) of the pore-grain interface is calculated from the two-point correlation function (Berryman, 1998).

$$S'_2(0) = -s / 4$$

The pore-pore two-point correlation function, S2(x, y), describes the probability that two points with a specified distance apart (a line) are both in pore phase. It is defined by:

$$S_2(x,y) = [f_{(i,j)}f_{(i+x,j+y)}] = 1/M.N \sum f_{(i,j)}f_{(i+x,j+y)}$$

In this study we have used a MATLAB built in function called "xcorr2" to calculate two-point correlation in the Cartesian coordinate. The calculated two-point correlation function in the Cartesian coordinate system is then used to calculate the planar radial average in the polar coordinate system using a two-dimensional bilinear interpolation method. A written MATLAB function called "average" is used for this purpose. This function is planned to map the two-point correlation function from a Cartesian coordinate system to polar coordinate system and then taking average along fixed radiuses. The input to the function is just the normalized two-point correlation function. The output is a vector that represents the average values of two-point correlation function along the fixed radiuses.

5 Results

5.1 Experimental Results

5.1.1 Gamma-Ray analysis

Collected data from three Gamma-Ray analyses were converted to photo (Figure 5-1) by Matlab program. By using a Matlab code measured attenuation has been converted to the range of colour from blue to the red in a way that red colour represents the low attenuation rate (less density or free spaces) and blue colour represents the high attenuation rate (denser areas like deformation bands).

Table 5-1 shows test configuration for gamma scan. The first configuration with short integration time and big scanning step resulted in rough visualization where the deformation bands are not recognizable. Based on test configuration, for the dry sample integration time is chosen to be 10s with the scanning steps of 1 mm. Then, we have good quality of visualization for composition of dry sample. Saturated sample is scanned under 1 mm scanning step but with higher integration time (20s) because, saturated sample absorbs more radiation and causes more attenuation.

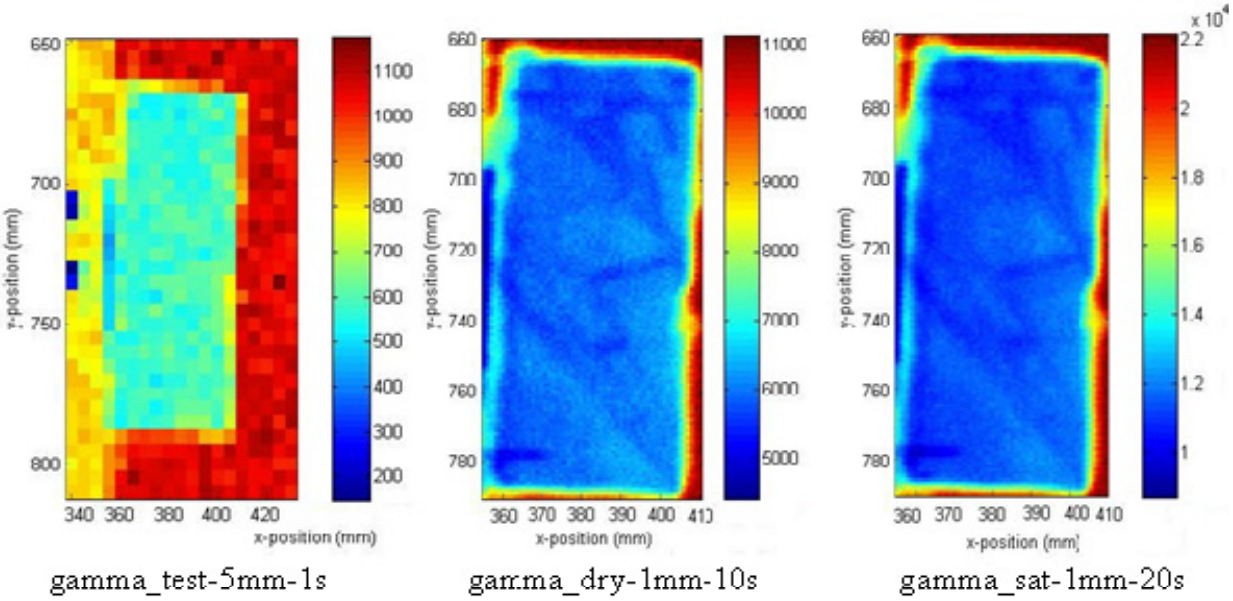

Figure 5-1: Gamma-Ray images(counts) for different configuration

Table 5-1: Test configuration for gamma measurement.

Experiment condition	X-range (mm)	Y-range (mm)	Integ. time (S)	Steps (mm)	Valve 1	Valve 2	Valve 3	Valve 4
test	340 - 430	430 -810	1	5	close	open	close	open
dry	355 - 660	410 - 790	10	1	close	open	close	open
saturated	355 - 660	410 - 790	20	1	close	open	close	open

5.1.2 Miscible displacement

Configuration of all tests (floods) is given in Table5- 2 as well as duration of each test.

Table 5-2: Test configuration for one phase injection.

Flood No.	Brine	Density (gr/lit)	Rate (ml/h)	Start (day time)	Duration (min)	Valve 1	Valve 2	Valve 3	Valve 4
1	NaCl	70	60	10.02.11 10.25	4	inlet	close	outlet	close
1	NaI	70	15	10.02.11 10.46	79	inlet	close	outlet	close
2	NaCl	70	60	10.02.11 13.15	86	inlet	close	outlet	close
2	NaI	70	15	10.02.11 14.46	84	close	Inlet	outlet	close
3	NaCl	70	60	10.02.11 16.23	67	close	Inlet	outlet	close
3	NaI	100	10	28.02.11 14:41	118	inlet	close	outlet	close
4	NaCl	100	60	03.03.11 14:51	69	inlet	close	outlet	close
4	NaI	100	10	03.03.11 16:24	80	outlet	outlet	close	inlet
5	NaCl	100	60	04.03.11 11.45	70	outlet	outlet	close	inlet
5	NaI	100	10	04.03.11 13.25	127	outlet	close	close	inlet

In the following figures the first and last X-Ray images of each flood is presented with a small picture of in/outlet configuration. Blocking of brine flow by deformation bands is visible in the figures (image labelled as last). The two different brines used in experiment can be distinguished where the doped brine is reckonable with darker area in photos and NaCl is lighter (almost same as dry sample). doped brine solvent with higher density (100 gr/lit) is shown even darker than solvent with 70 gr/lit density. Effect of different density and injection rate is comparable in NaI floods 1 and 3; the time used for flooding of brine with higher density and lower injection rate is relatively longer.

Flood 1-Displacement of NaCl brine by doped brine

First, the sample is saturated with NaCl (7% density) and it is made ready for the first NaI flood which is darker. Figure 5-2 shows first and last images of X-Ray series taken during imbibition. The brine is clear, therefore, no special change is seen in two images.

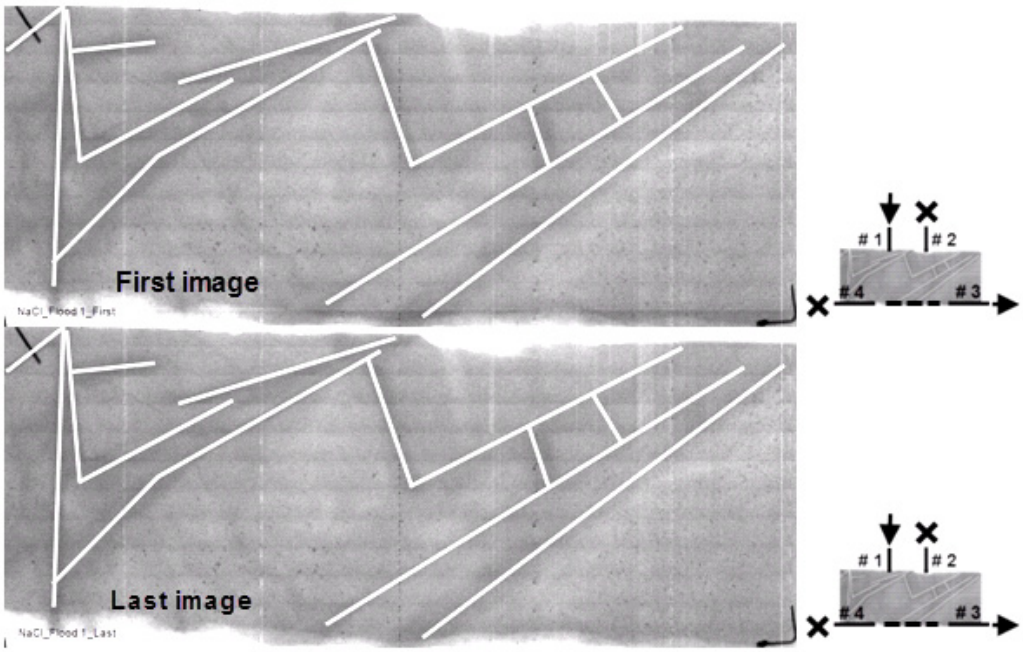

Figure 5-2: Flood 1, First and last image of imbibition with NaCl: density: 7%, rate: 60 ml/h, time: 4 min.

Flood 1- Injecting NaI

Main visualizing brine which is NaI with 7% density is injected into the sample in this step. The rate of injection is chosen to be lower in order to have better screening of flooding. Injection is stopped after 79 minutes where no more special changes are observed in the last four images. Figure 5-3 shows first and last image of this series and it is easy to compare sample before and after flood; deformation bands are marked as white line in this figure.

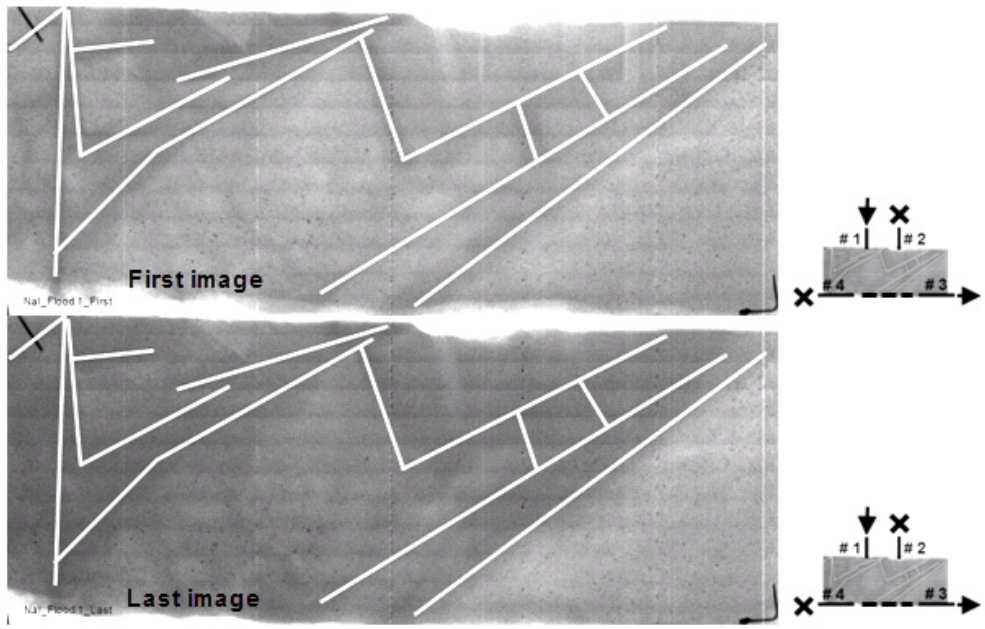

Figure 5-3: Flood 1, First and last image of NaI injection, density: 7%, rate: 15 ml/h, time: 79 min.

Also the sequence of fluid flow is illustrated in Figure 5-4_a&b with details of time, volume and percentage of filled pore area. We can observe how deformation bands obstruct and redirect the flow. In the absence of deformation bands we expect an even distribution of flow in sample radiating from valve#1 and exiting from valve#3 after replacing NaCl in the entire or recognizable part of the sample.

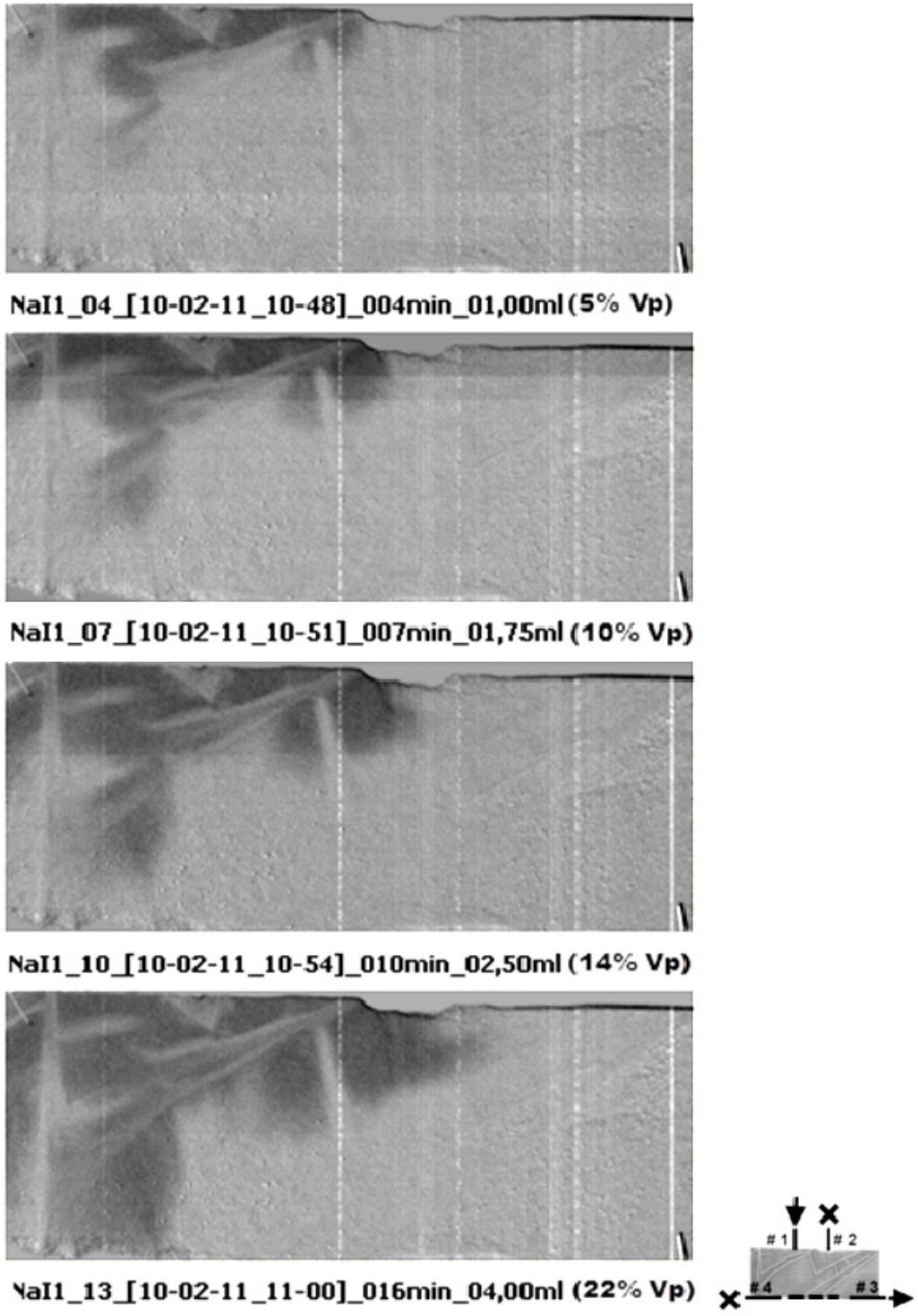

Figure 5-4_a: One phase, Flood 1, Sequence of NaI injection (70g/L, 15ml/h, 79 min).

However, deformation bands affect the flow pattern, especially in right-lower part of images (Figure 5-4_a&b), they do not allow the fluid to pass and reach directly the exit valve. The NaI enters the bottom groove and then exit from valve#3.

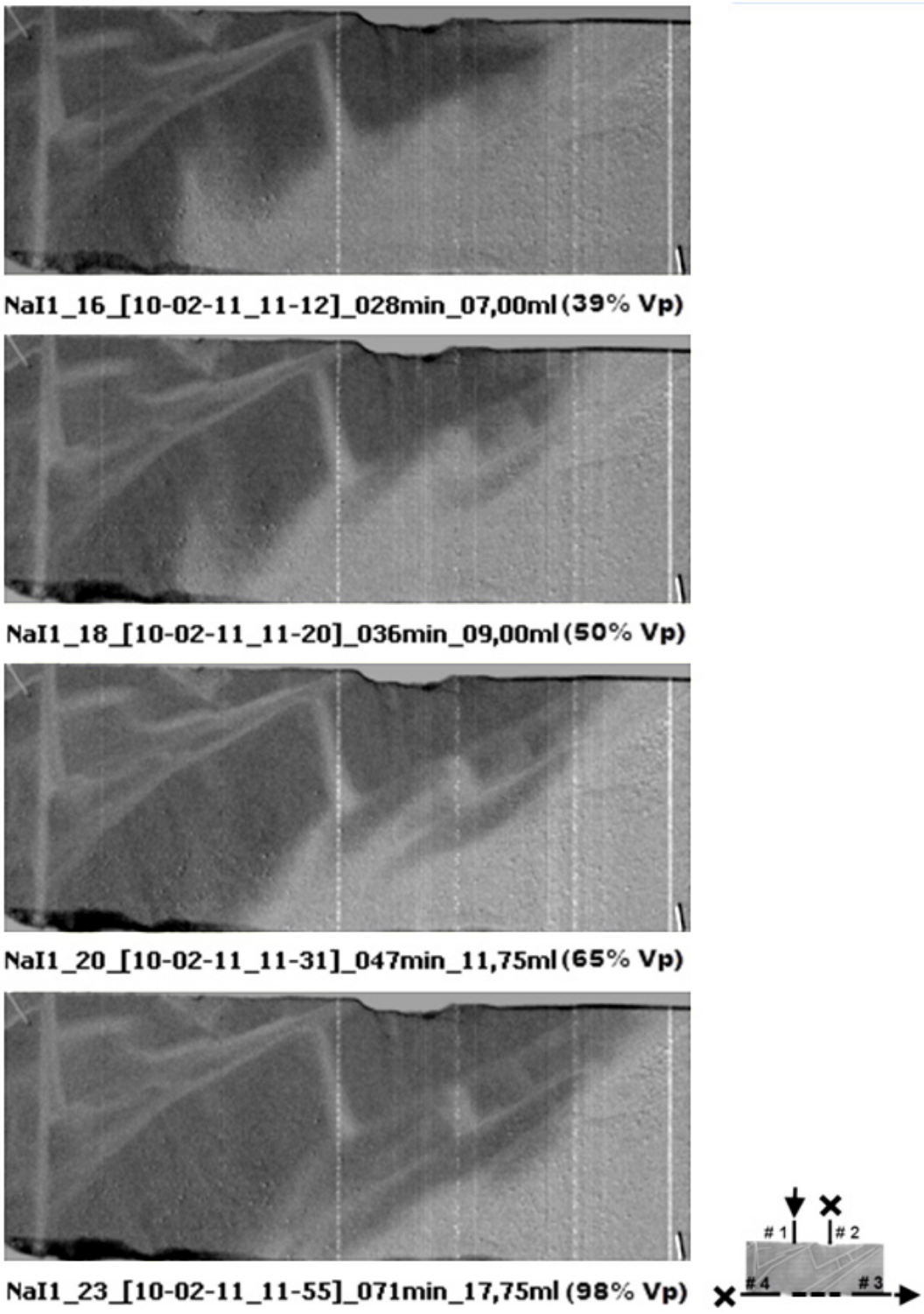

Figure 5-4_b: Continue of one phase, Flood 1, Sequence of NaI injection (70g/L, 15ml/h, 79 min).

Flood 2- Displacement of doped brine by brine

The sample is made ready for next NaI flood by draining existing brine with NaCl. The time of injection is decided to be longer to make sure that sample is clear of NaI and filled with NaCl (Figure 5-5).

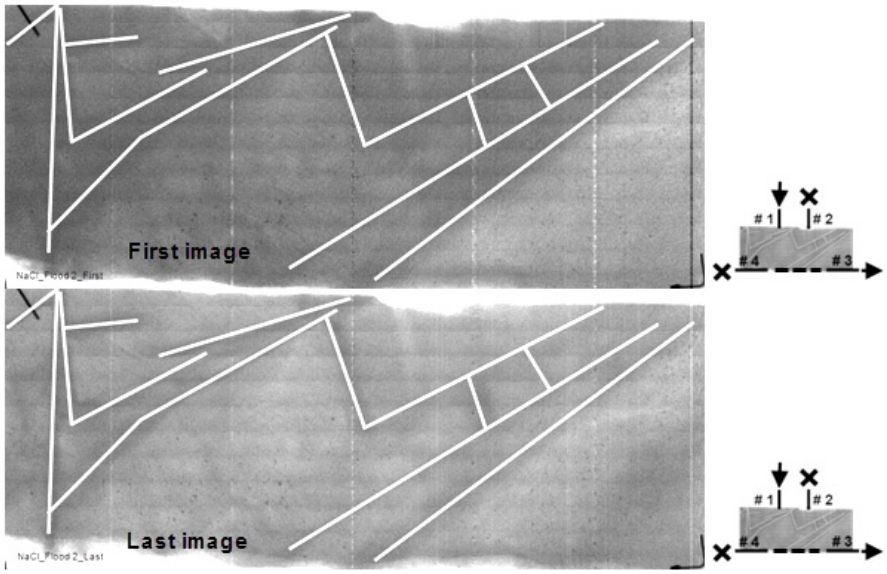

Figure 5-5: Flood 2, First and last image of imbibition with NaCl: density: 7%, rate: 60 ml/h, time: 86 min.

Flood 2- Injecting NaI

With the new configuration (valve#2 as input) the second NaI flood was performed and as it is detectable in Figures 5-6 and 5-7_a&b, deformation bands redirect the fluid flow to bottom groove and exit valve before allowing a smooth distribution of brine in the sample; especially in the left side of sample where there is no flow area inside and behind bands.

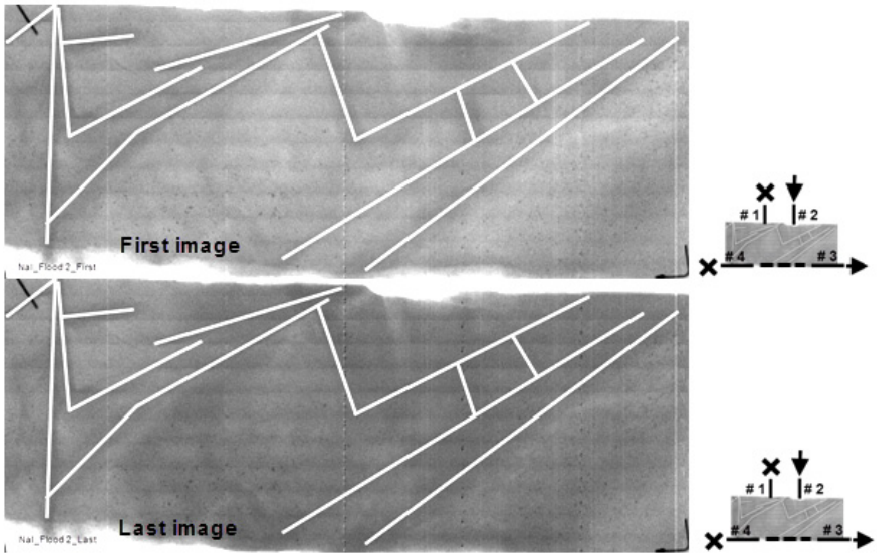

Figure 5-6: Flood 2, First and last image of NaI injection, density: 7%, rate: 15 ml/h, time: 84 min.

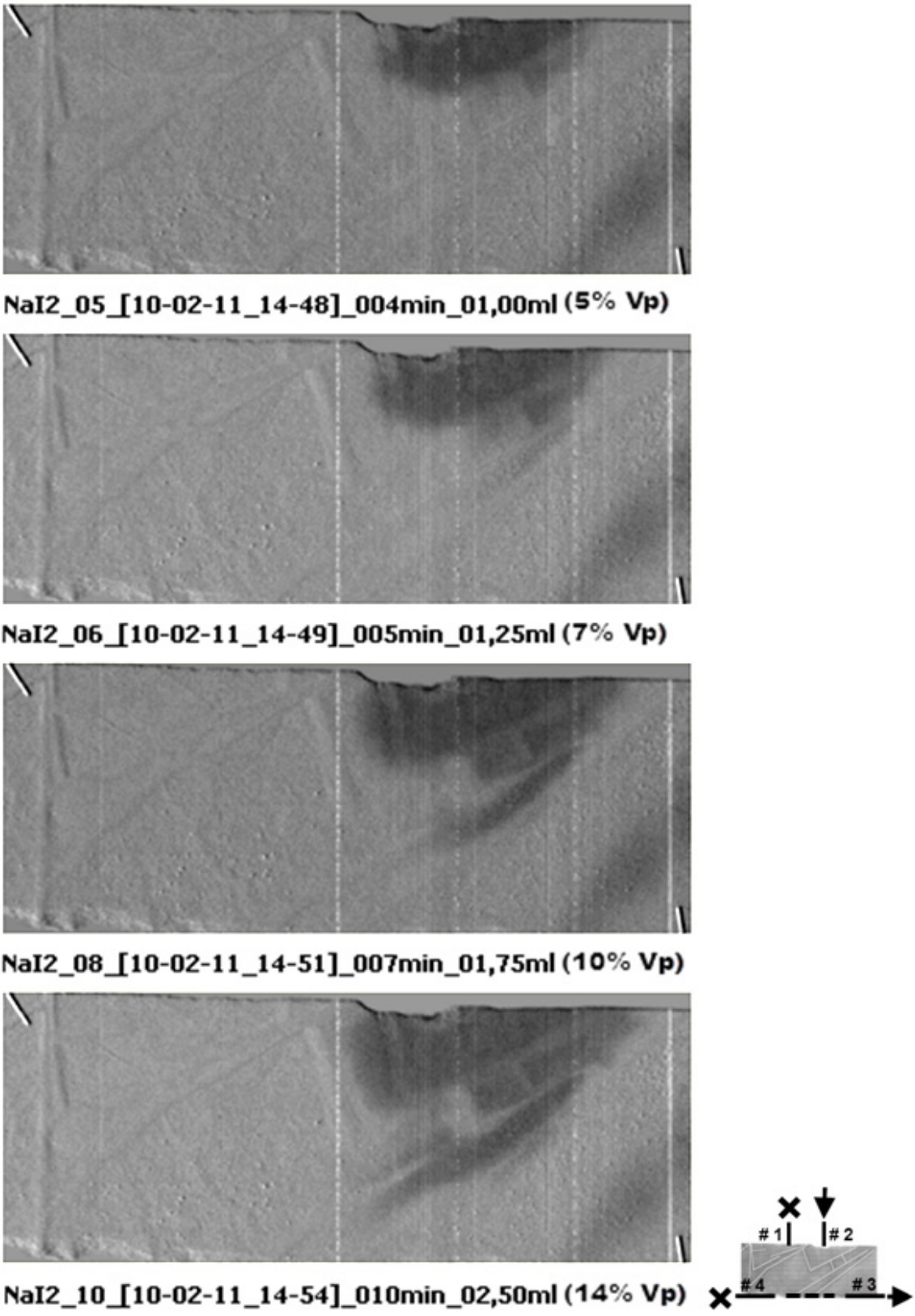

Figure 5-7_a: One phase, Flood 2, Sequence of NaI injection (70g/L, 15ml/h, 84 min).

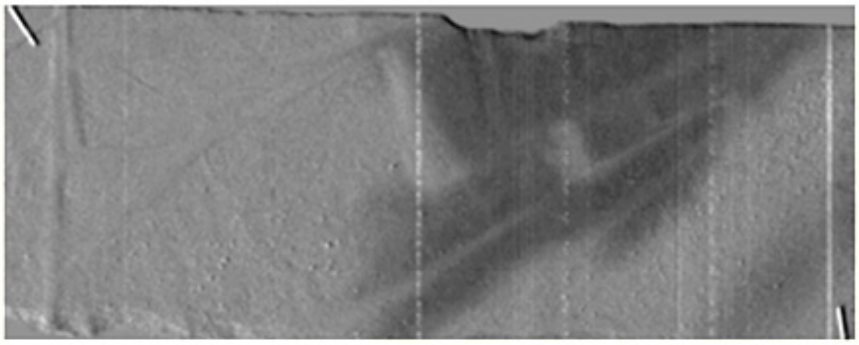

NaI2_12_[10-02-11_15-00]_016min_04,00ml (22% Vp)

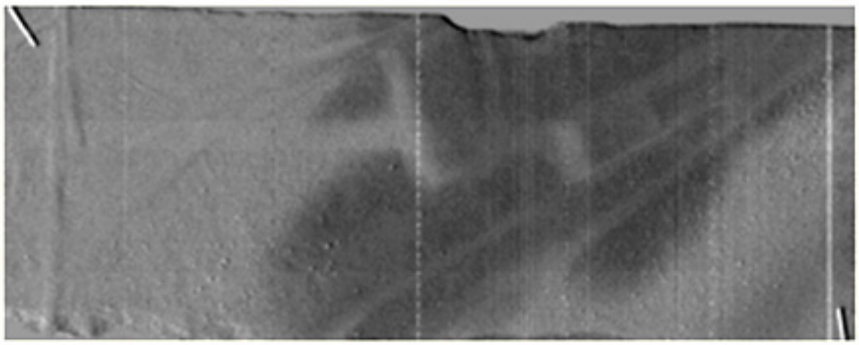

NaI2_14_[10-02-11_15-11]_027min_06,75ml (37% Vp)

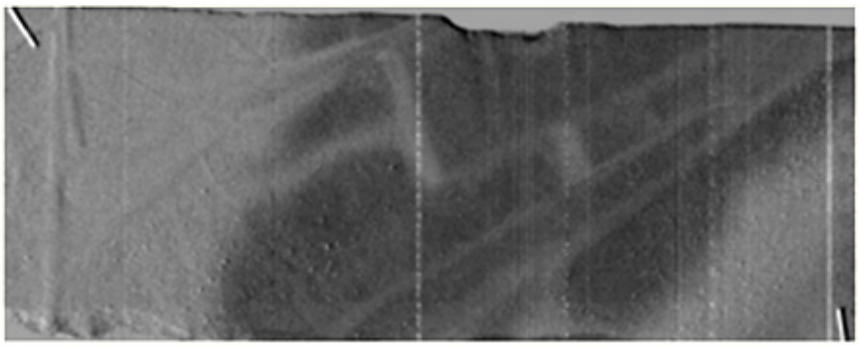

NaI2_16_[10-02-11_15-26]_042min_10,50ml (58% Vp)

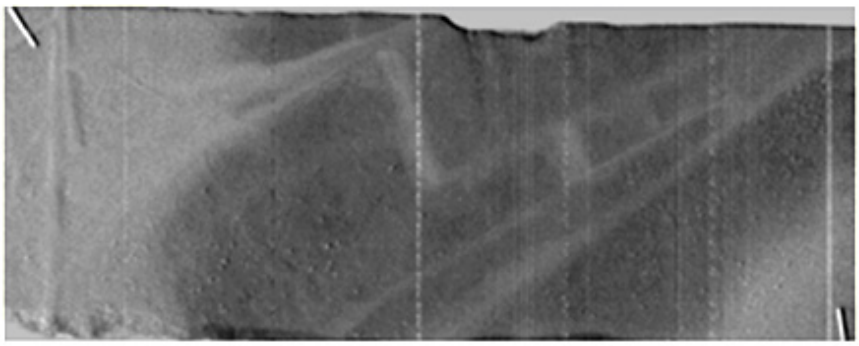

NaI2_19_[10-02-11_15-55]_071min_17,75ml (98% Vp)

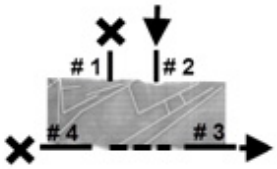

Figure 5-7_b: Continue of one phase, Flood 2, Sequence of NaI injection (70g/L, 15ml/h, 84 min).

Flood3- Draining NaI by injecting NaCl

NaI was removed from sample by injecting NaCl. It took 67 minutes to have sample filled with NaCl as it is shown in Figure 5-8.

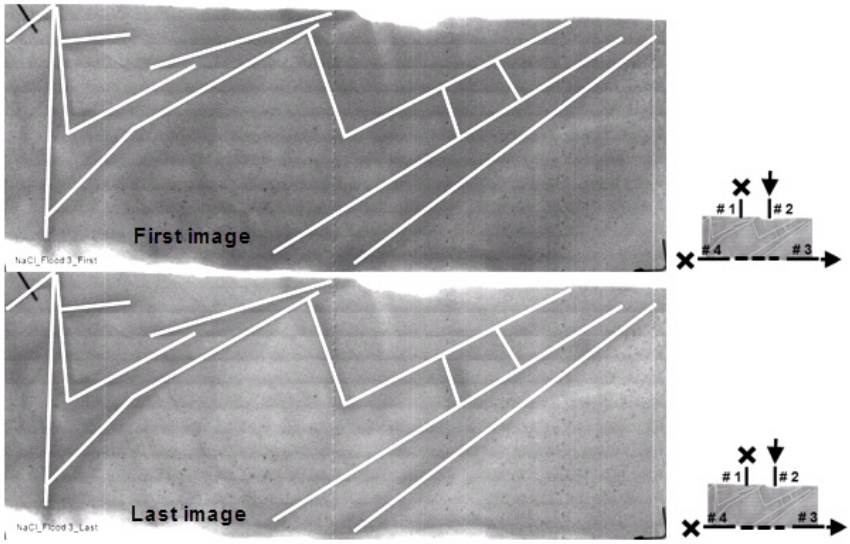

Figure 5-8: Flood 3, First and last image of imbibition with NaCl: density: 7%, rate: 60 ml/h, time: 67 min.

Flood 3- Injecting NaI

The third NaI flood is almost the same as the first one with the same valve configuration but different brine density (10%) and slower injection rate (10 ml/h) which resulted in longer injection time comparing to flood 1. This test was conducted to observe the effect of brine density and injection rate and as it is observed in Figures 5-9 to 5-10_a&b the flow pattern is very similar to flow pattern in flood 1.

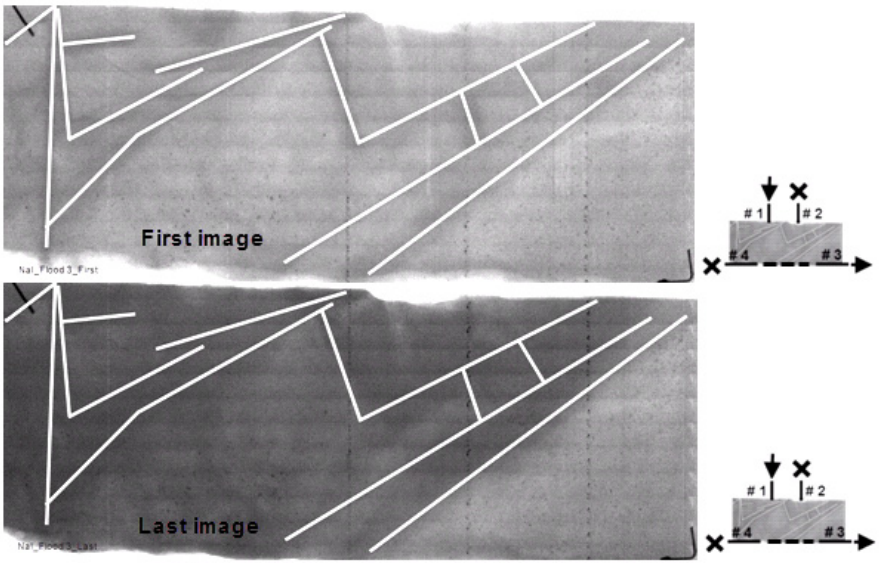

Figure 5-9: Flood 3, First and last image of NaI injection, density: 10%, rate: 10 ml/h, time: 118 min.

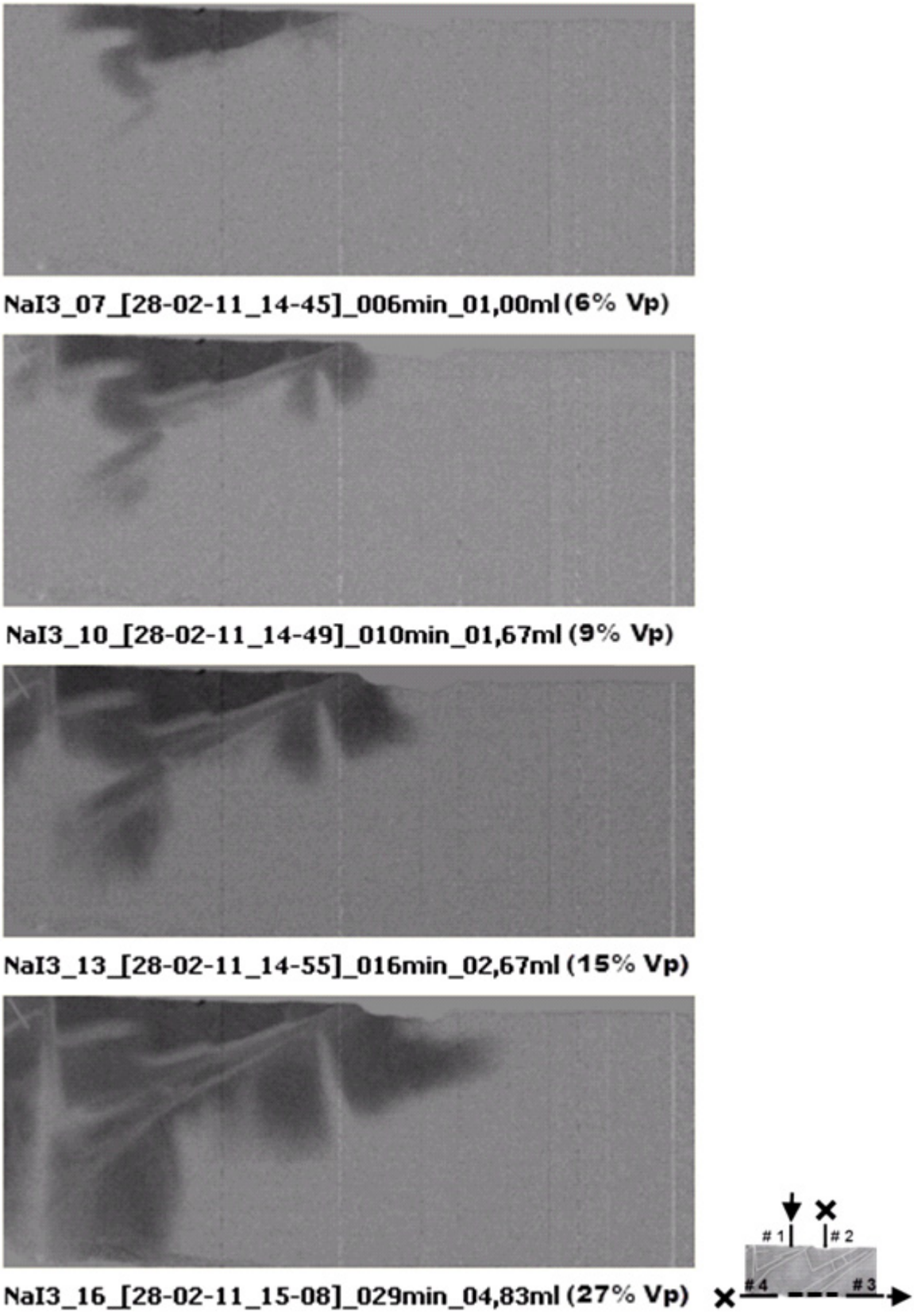

Figure 5-10_a: One phase, Flood 3, Sequence of NaI injection (100g/L, 10ml/h, 118 min).

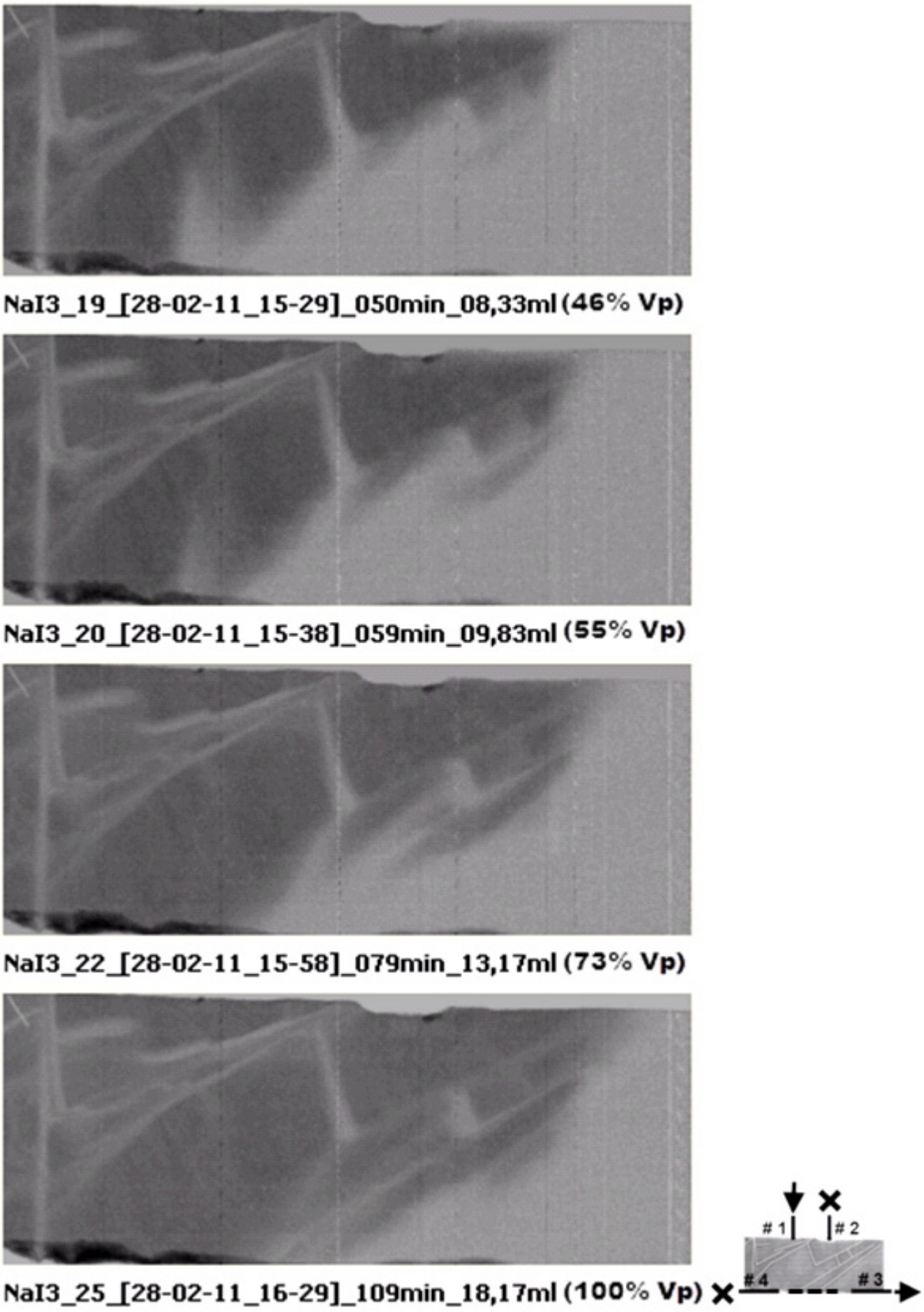

Figure 5-10_b: Continue of one phase, Flood 3, Sequence of NaI injection (100g/L, 10ml/h, 118 min).

Flood4- Draining NaI by injecting NaCl

In this part sample was prepared for next injection by replacing NaI with 10% density NaCl and the rate of 60 ml/h. It took 69 minutes to remove NaI from the sample observing no major change in images after this time (Figure 5-11).

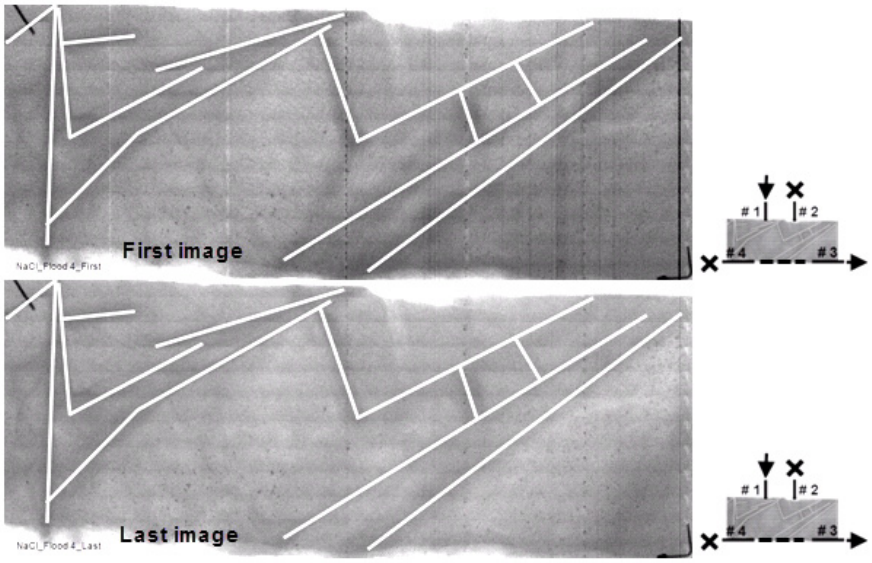

Figure 5-11: Flood 4, First and last image of saturation with NaCl: density: 10%, rate: 60 ml/h, time: 69 min.

Flood 4- Injecting NaI

New configuration of valves is chosen to have 2 outlets (#1 & #2) and valve #4 works as inlet. Brine density and injection rate are chosen to be same as Flood 3 (10% and 10 ml/h). 80 minutes injection of brine was needed to have stable flow pattern in images (Figure 5-12).

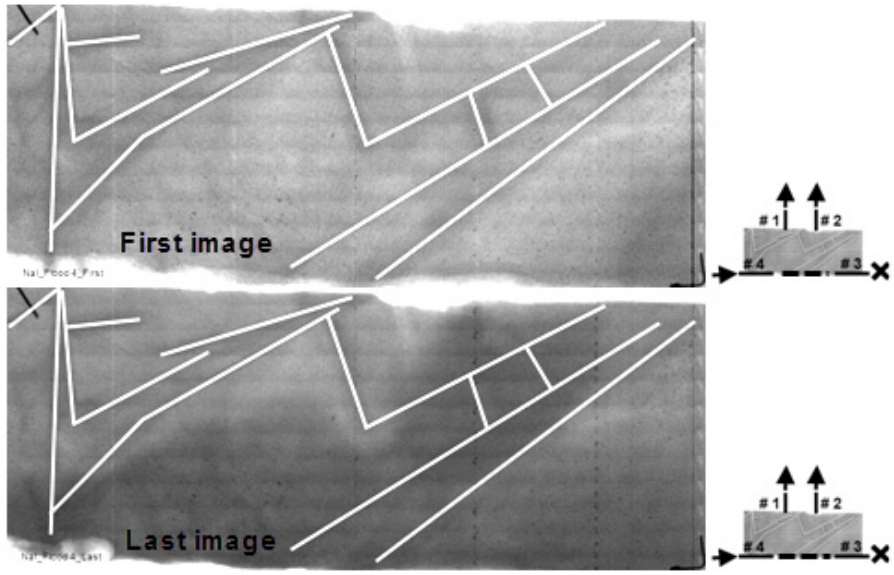

Figure 5-12: Flood 4, First and last image of NaI injection, density: 10%, rate: 10 ml/h, time: 80 min.

In this test two of diagonal deformation bands (middle-right) and the area between them seem to conduct the fluid flow in their longitudinal direction toward outlet#2 whereas the deformation bands in left side of image worked as barrier and prevent the fluid from reaching the outlet#1. The sequence and how the bands act is shown in Figures 15-13_a&b.

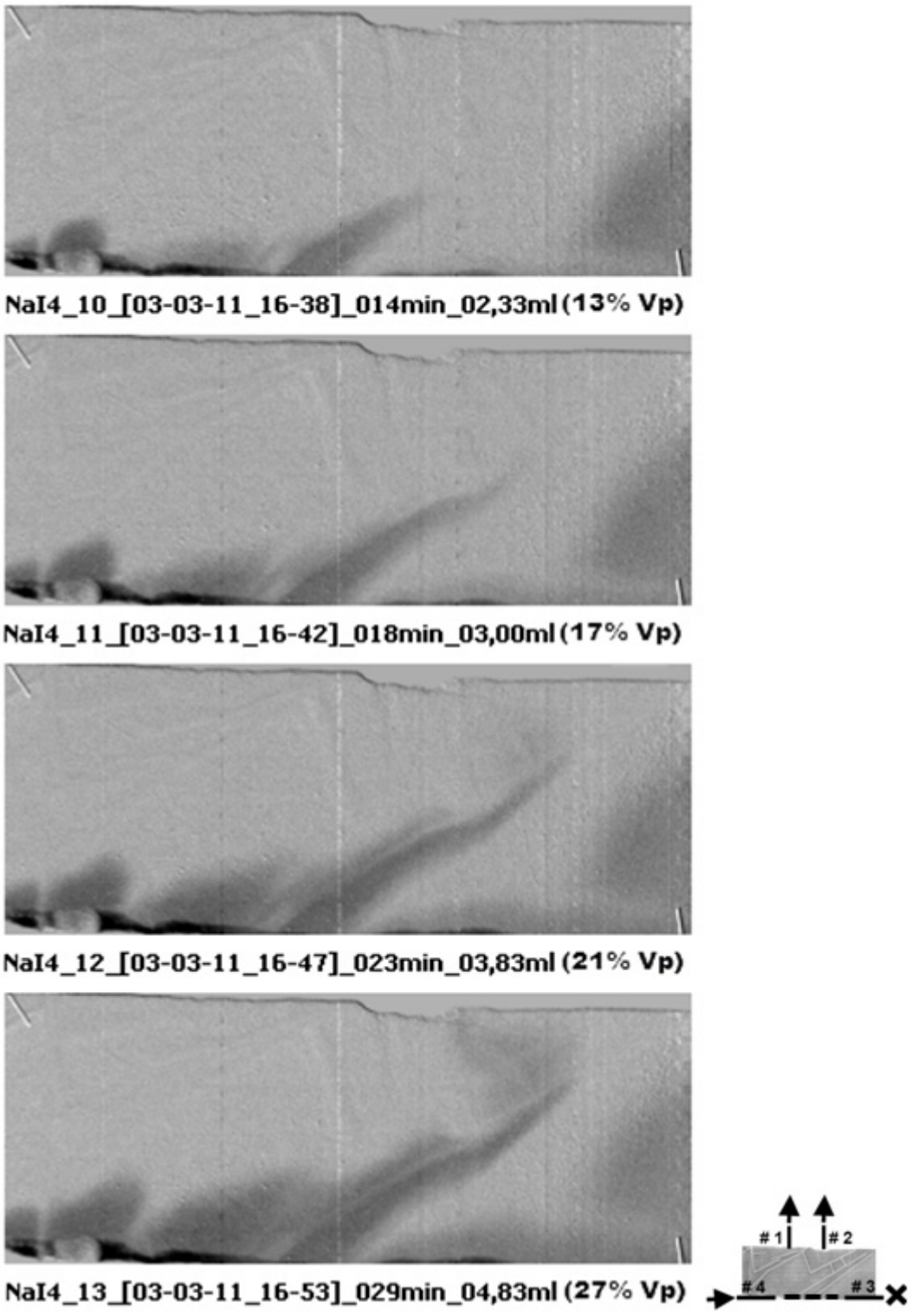

Figure 5-13_a : One phase, Flood 4, Sequence of NaI injection (100g/L, 10ml/h, 80 min).

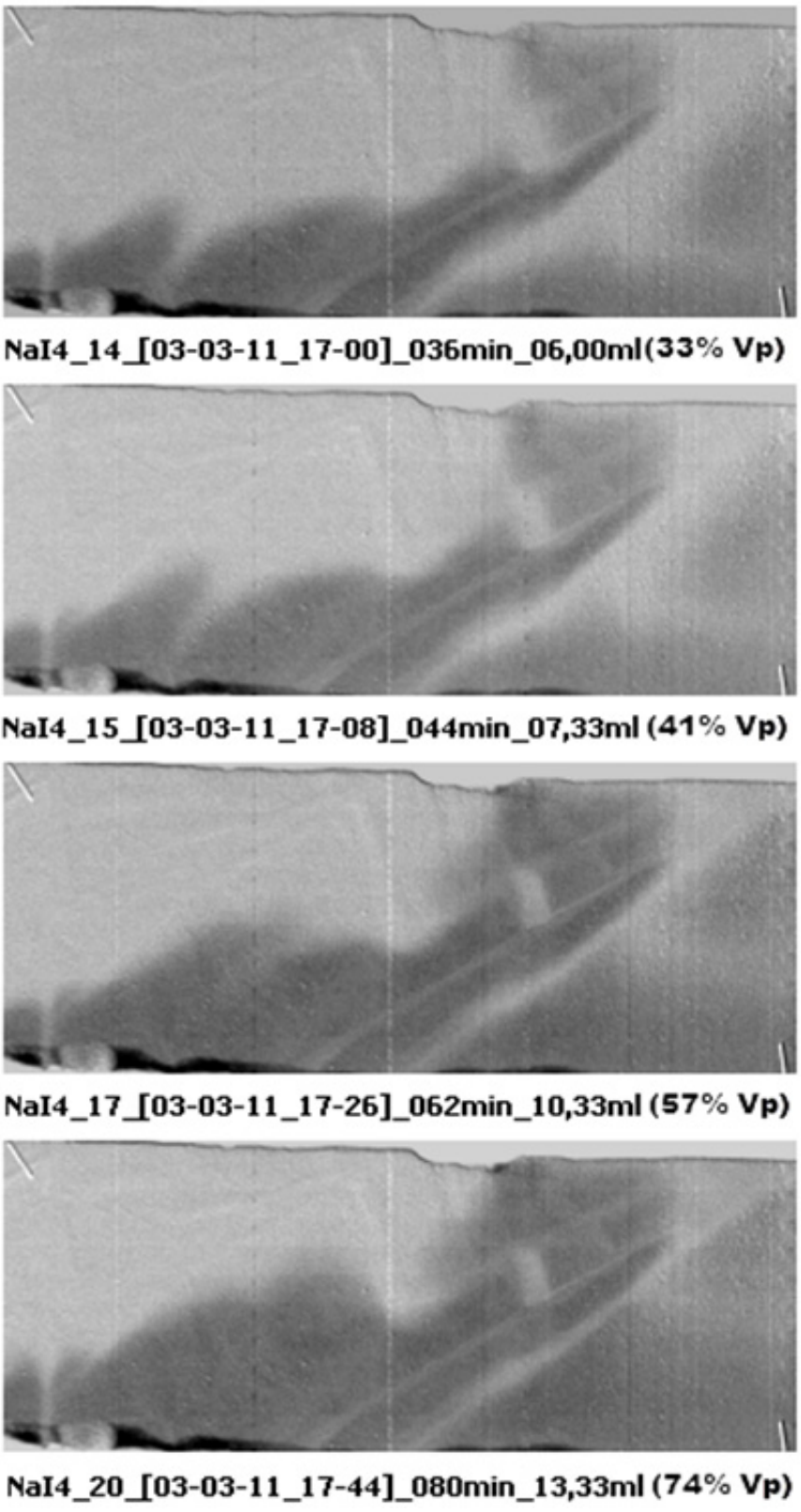

Figure 5-13_b: Continue of one phase, Flood 4, Sequence of NaI injection (100g/L, 10ml/h, 80 min).

Flood 5- Removing NaI by injecting NaCl

The sample was prepared for next NaI injection by replacing NaI with 10% NaCl during 70 minutes. Figure 5-14 shows sample before and after this injection.

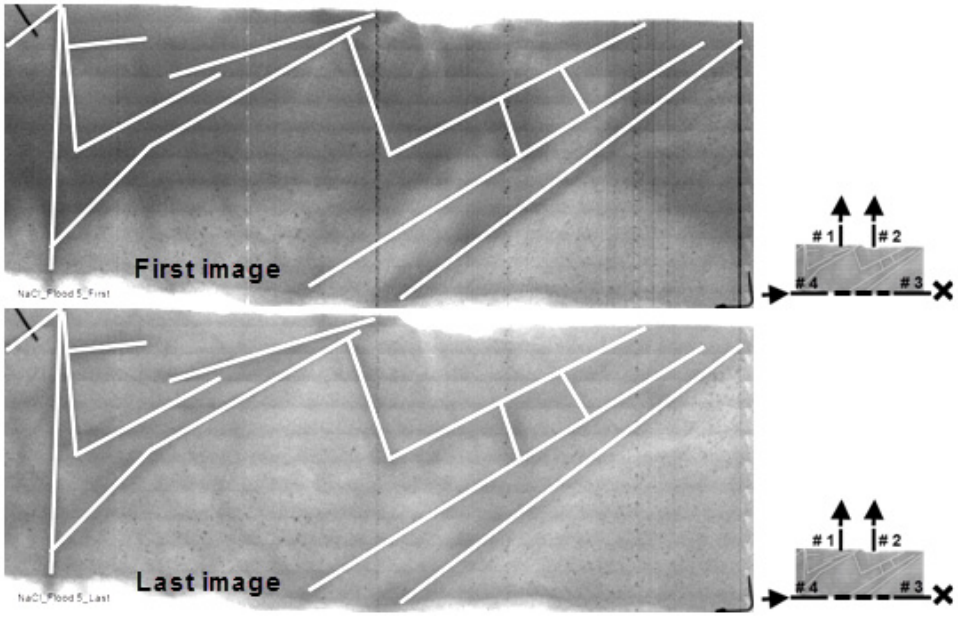

Figure 5-14: Flood 5, First and last image of imbibition with NaCl: density: 10%, rate: 60 ml/h, time: 70 min.

Flood 5- Injecting NaI

Last test was conducted with similar configuration as flood 4, except valve #2 which was kept closed in this flood to investigate the boundary (outlet) effect on fluid flow in the sample and the interaction with the effect of deformation bands (Figure 5-15).

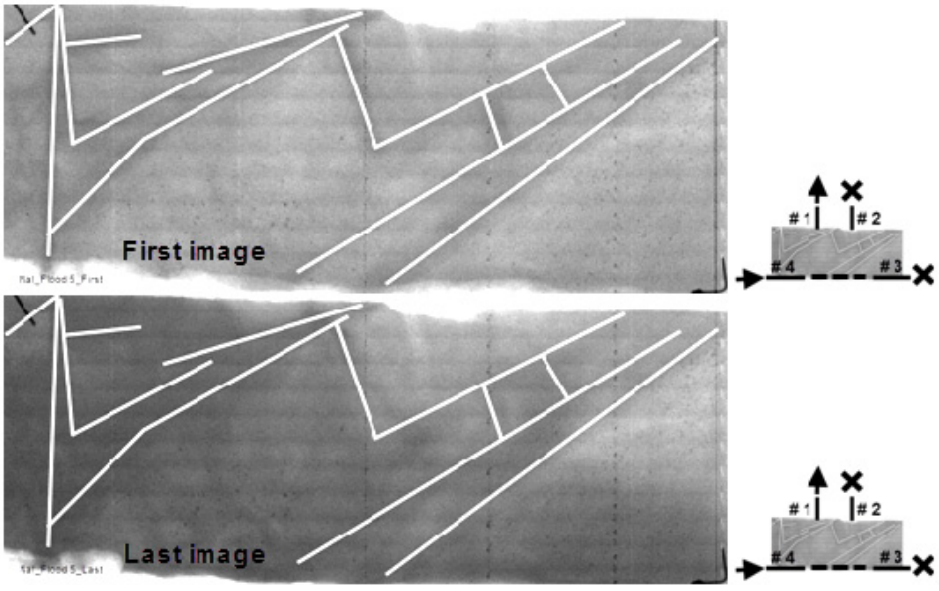

Figure 5-15: Flood 5, First and last image of NaI injection, density: 10%, rate: 10 ml/h, time: 127 min.

By studying Figure 5-16_a&b we observe how fluid chooses the shortest way to the single outlet where the valve#2 is kept closed. On the other hand, on the way to the outlet flow is affected by deformation bands; the band parallel to width of sample facilitates the flow along itself.

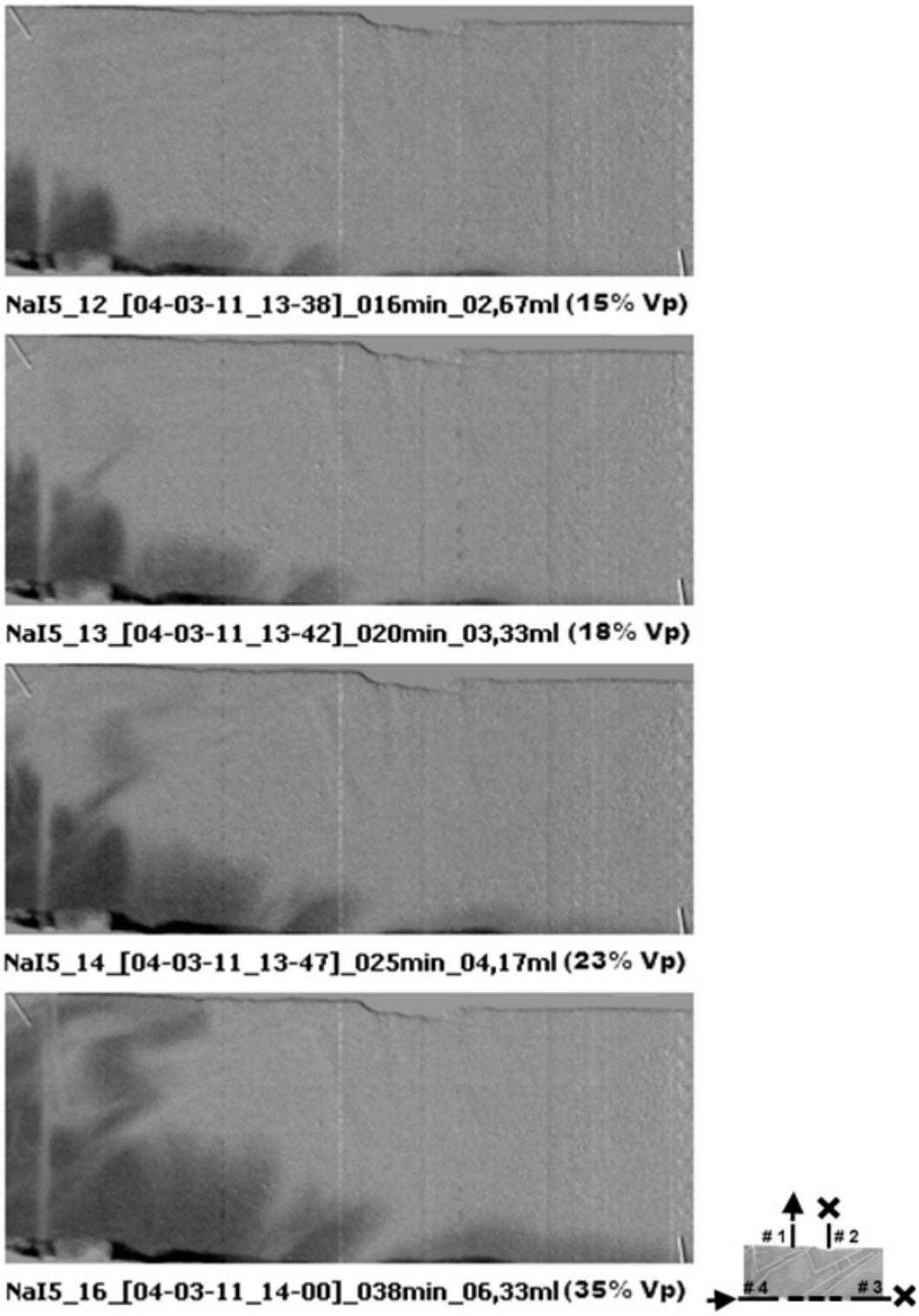

Figure 5-16_a: One phase, Flood 5, Sequence of NaI injection (100g/L, 10ml/h, 127 min).

Flow is also affected by diagonal bands being redirected between them to reach outlet#1. Furthermore, these diagonal bands hinder the expected even distribution of brine and delay the fluid flow in the sample.

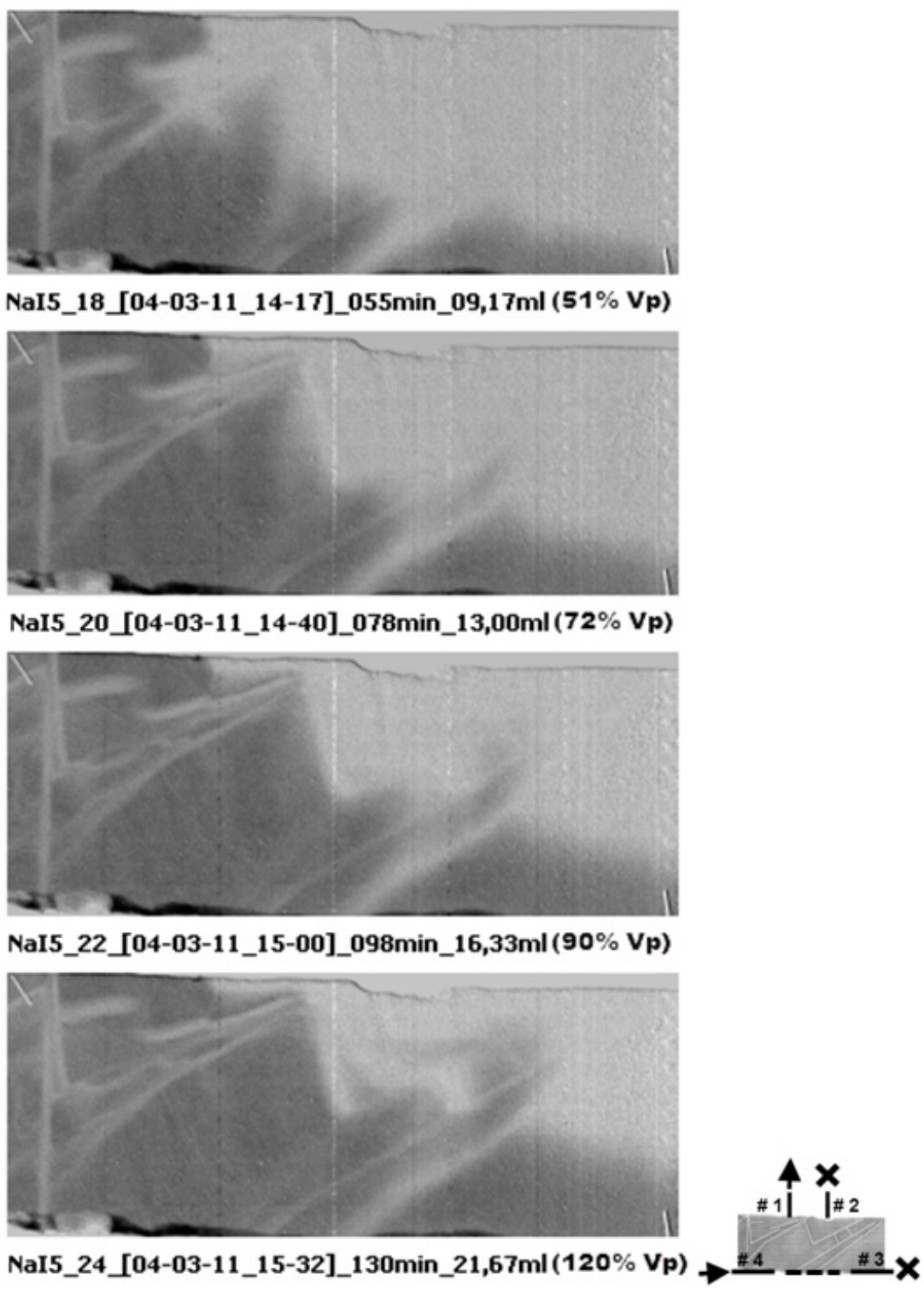

Figure 5-16_b: One phase, Flood 5, Sequence of NaI injection (100g/L, 10ml/h, 127 min).

5.1.3 Two phase injection

Table 5-3: Detail and configuration of two phase injections.

Flood No.	Type	Brine	Density (gr/lit)	Rate (ml/h)	Duration (min)	Configuration
1	imbibition	NaI	100	20	120	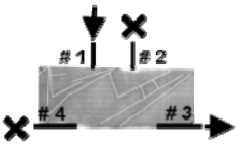
2	imbibition	NaI	100	20	120	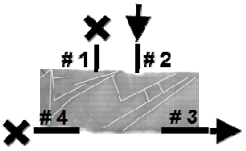
3	drainage	Decane		10	59	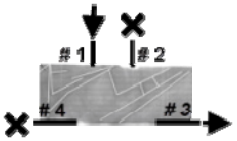
4	drainage	Decane		10	79	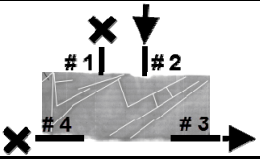

Imbibition

NaI solvent with density of 100g/L is used as water phase and the sample is saturated in two steps from inlet 1 and 2 while valve 3 was outlet and respectively valve 2 & 4 and 1 & 4 were kept closed (Table 5-3). The injection in each arrangement took 2 hours and the rate chosen to be lower than one phase tests as 20 ml/h to make sure that sample is fully saturated with NaI.

Drainage:

Draining NaI by injecting Decane was repeated with the same sequence and valve arrangements for imbibition. Following figures (5-17 to 5-18) illustrate how Decane is moving out the brine. While injecting the fluids, the volume of injected and collected fluid was measured; making possible to calculate porosity, production water and saturations.

During flood 3 Decane which is observable as lighter colour in sample is replacing brine in the area behind the intersected deformation bands in the way that mostly upper half of the

sample is saturated by Decane, but the replacement is not improved after 1 hour, therefore we shift the inlet port and continue draining.

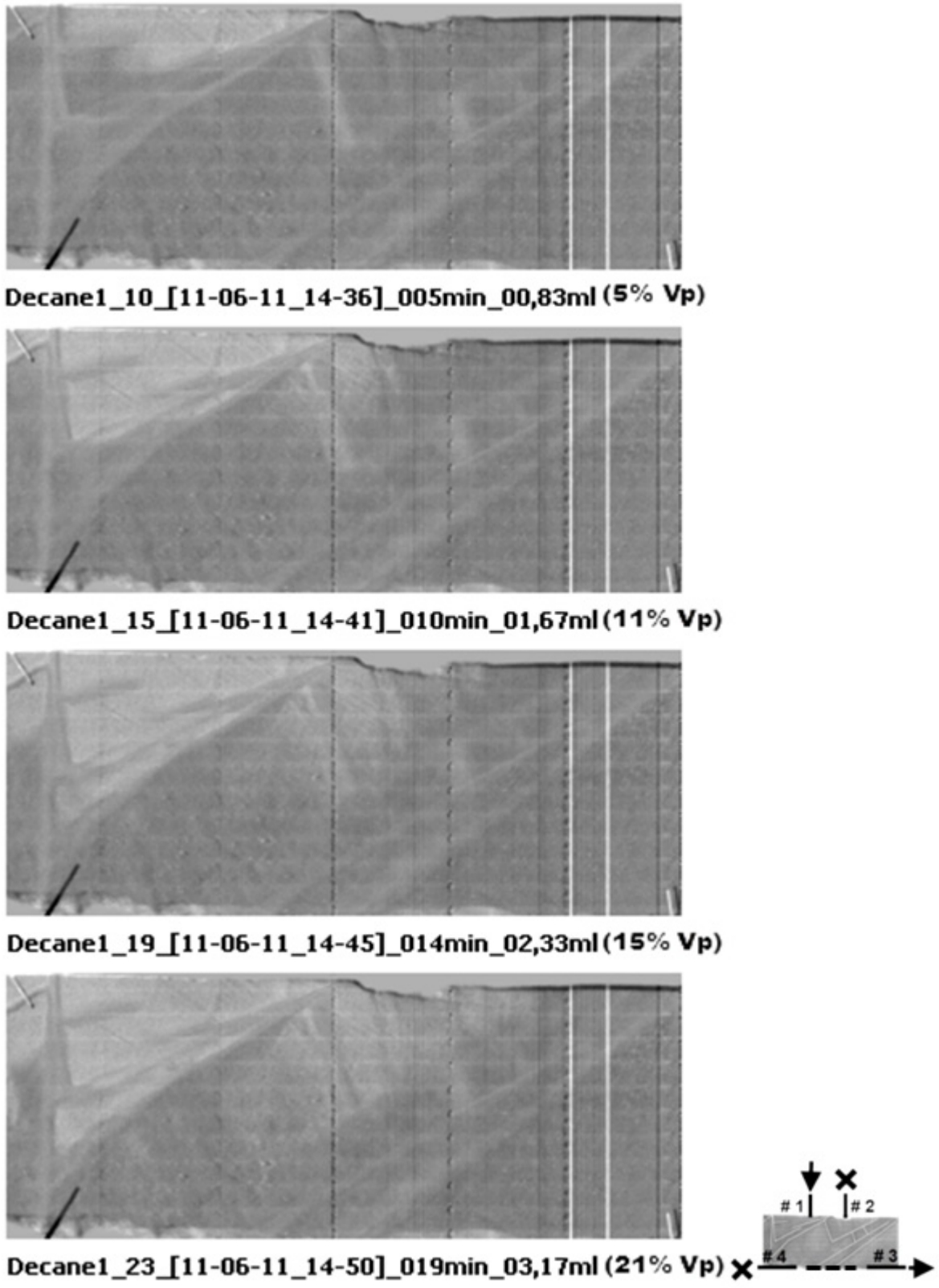

Figure 5-17_a: Two phase, Flood 3, Sequence of Decane injection (10ml/h, 59 min).

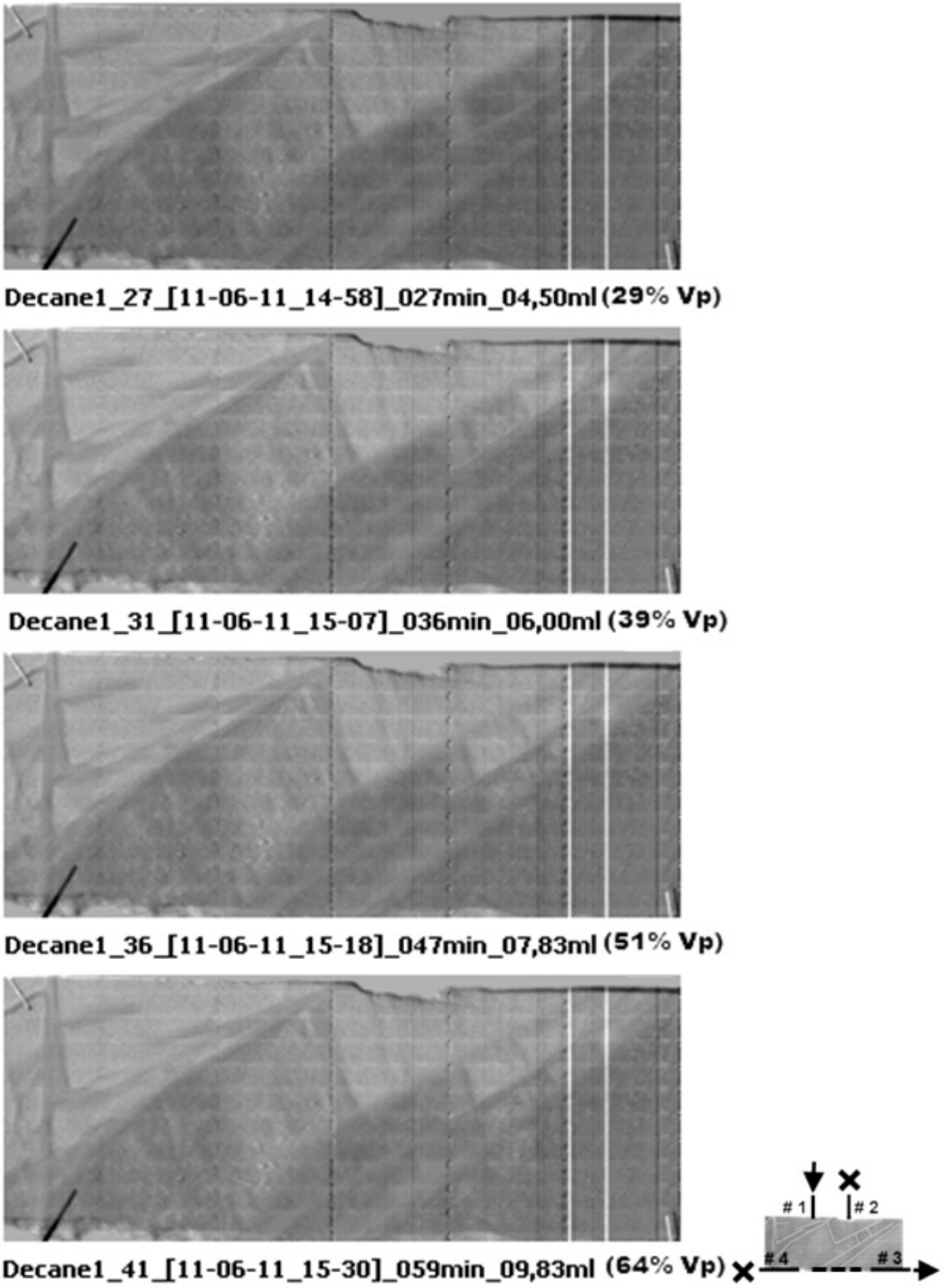

Figure 5-17_b: Continue of two phase, Flood 3, Sequence of Decane injection (10ml/h, 59 min).

The second round of draining has been carried out while Decane was injected from port#2 and letting brine to exit from port#3. We observed that not all of the NaI volume is being drained and it seems that deformation bands increase the capillary pressure (Figures 5-24 and 5-25).

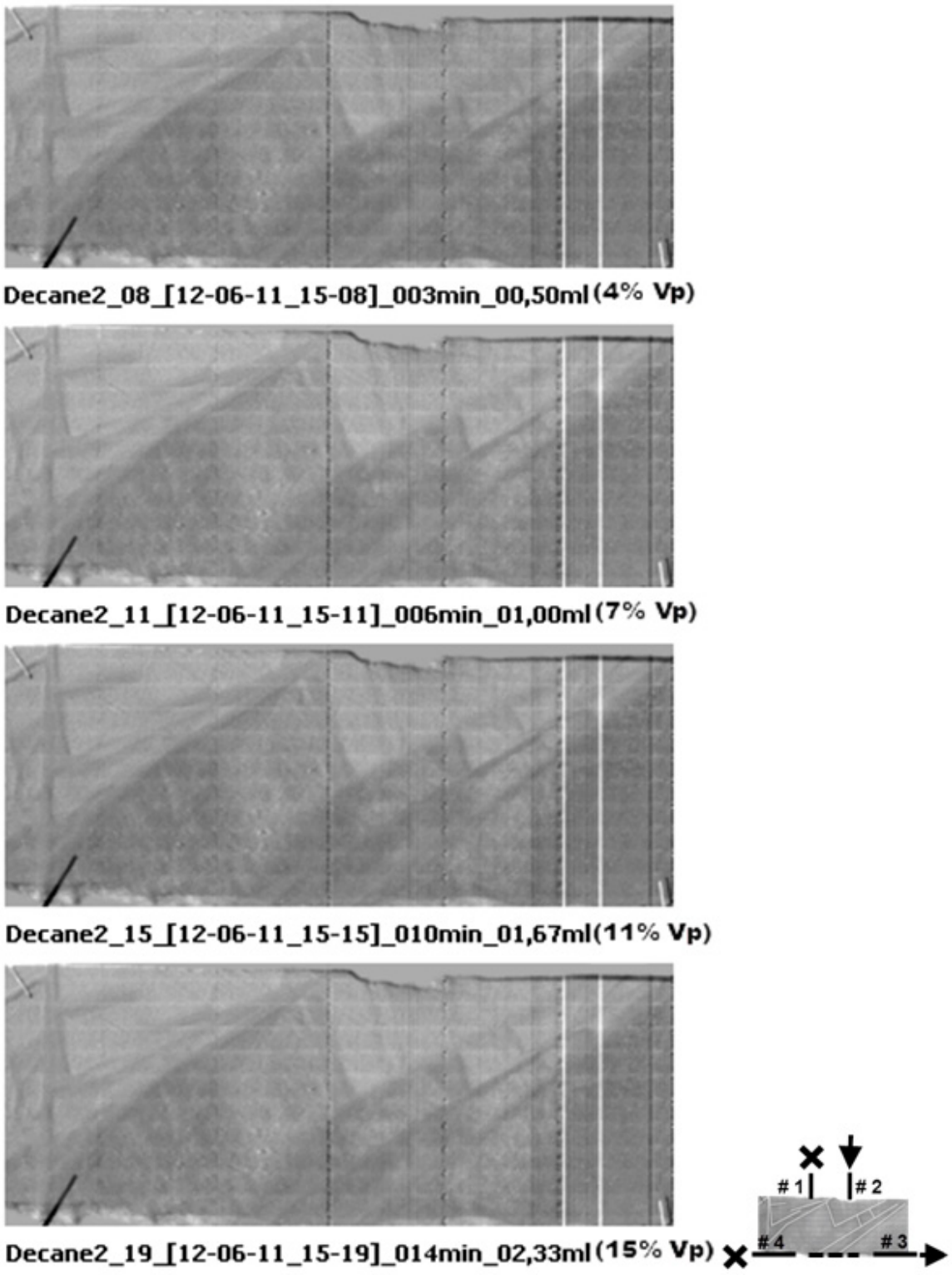

Figure 5-18_a: Two phase, Flood 4, Sequence of Decane injection (10ml/h, 79 min).

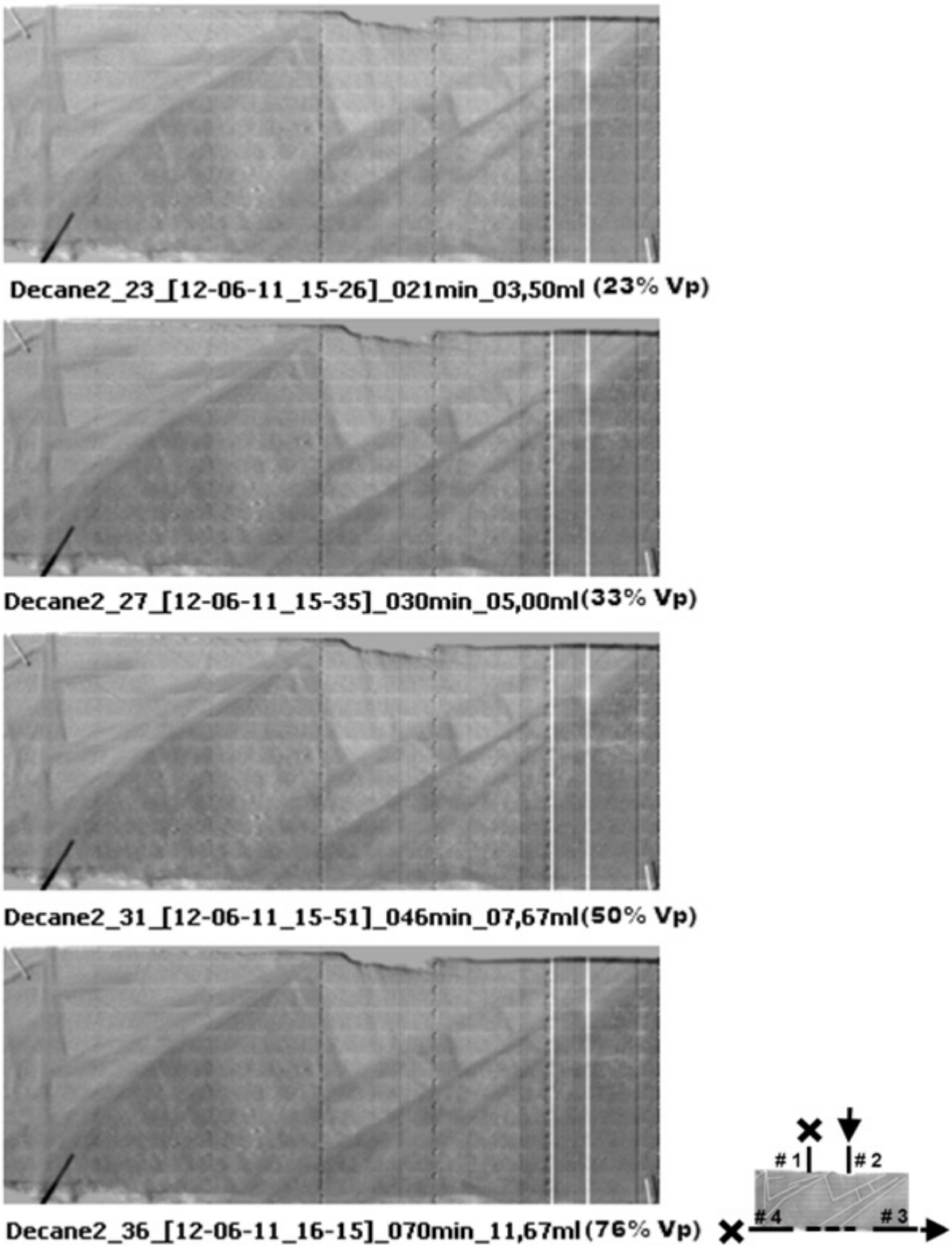

Figure5-18_ b: Two phase, Flood 4, Sequence of Decane injection (10ml/h, 79 min).

5.1.4 Porosity & Saturation

Saturation in the sample in each phase has been estimated for this part of experiment using volume of injection performed during experiment. Volume of the sample is estimated earlier in methodology section based on direct dimension measurement as 71736 mm^3 (49x122x12). Volume of injected NaI (15.3ml) is used to estimate pore volume of the sample. It is slightly different from which we measured in one phase test and it could be because of changing of sample properties during many injection, remaining some brine in sample or measurement's errors. Production water in first Decane flood (flood 3 in two phase experiments) was 5.8 ml, whereas the second Decane flood (flood 4 in this series) did not produce considerable volume of water and produced only 1 ml. Based on the above mentioned volumes, the porosity and saturations are calculated as below.

Porosity: 15300 mm^3 / 71736 mm^3 = 21%

Water saturation: (15.3 – 6.8) / 15.3 = 55%

Oil saturation: 6.8 / 15.3 = 45%

5.2 Microscopic Studies

Many optical and BSE images were taken from both thin sections; mostly on deformation bands. High resolution images were selected for estimation of porosity and permeability by image processing (Torabi et al. 2008). The list of images and the related estimated properties are shown in Table 8-1. Appendix includes all the images taken from thin sections. In addition, location of some selected areas for porosity and permeability estimation is illustrated in Figure 5-19.

Main purpose of property estimation on thin section images is to compare the porosity and permeability in deformation bands against host rock (or between bands). Moreover, it has done to investigate that if these results match the pervious experimental studies. Figures 5-20 & 5-21 are graphs that compare estimated porosity and permeability within deformation bands and host rock. They show that permeability in general has direct relation with porosity (higher porosity results in higher permeability), but not for all data. In addition, as we expected, both porosity and permeability is higher in the host rock and in the area between deformation bands comparing with porosity and permeability in deformation bands.

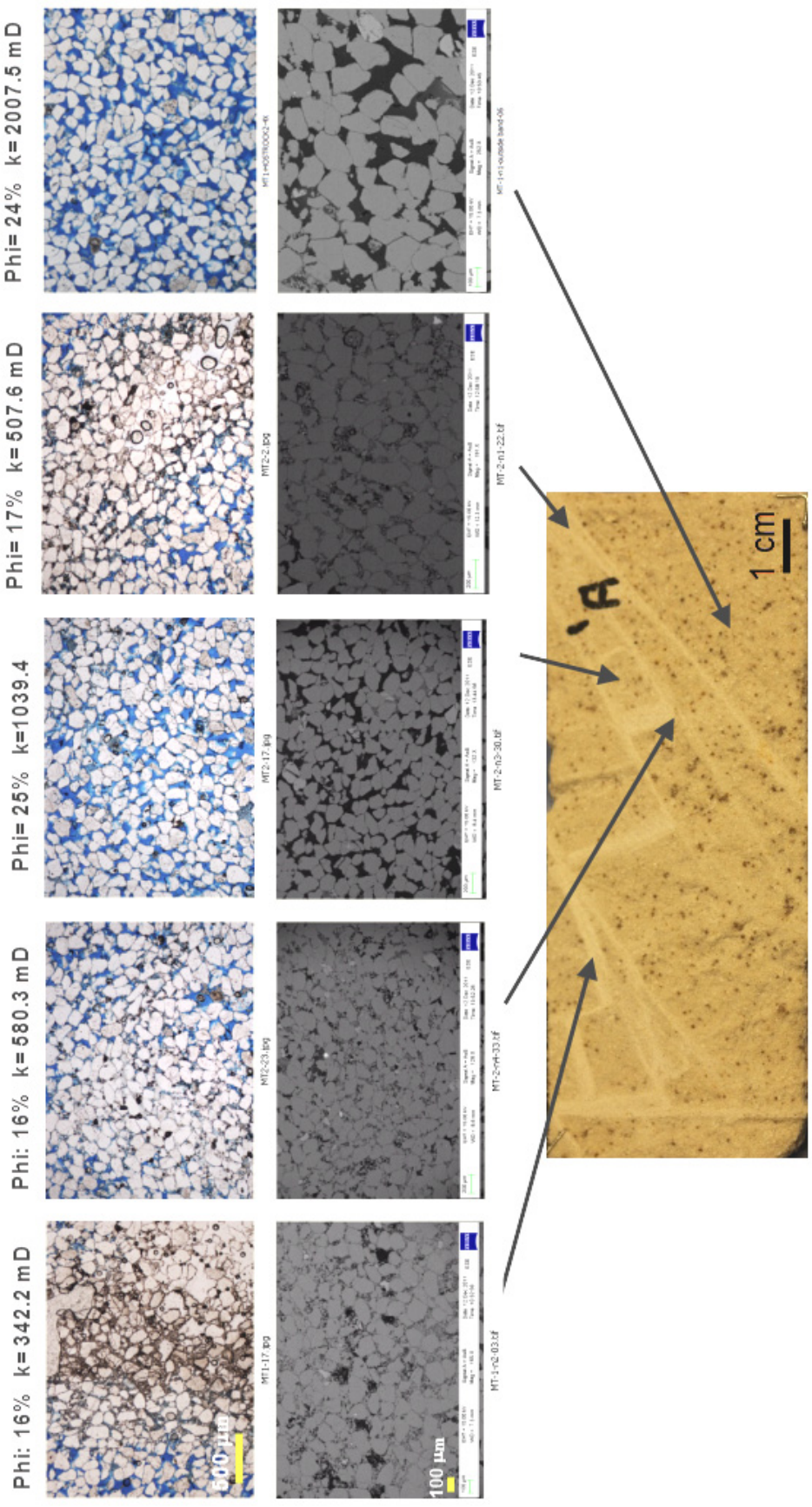

Figure 5-19: Location of some selected areas for porosity and permeability estimation.

Table 5-4: List of images used for porosity and permeability estimation and calculated parameters (DB refers to deformation band and HR to host rock).

Area	Photo	Position	pixels	Porosity	k (mD)
A	MT1-17.jpg	DB	I=I(1201:1800,1601:2200);	0.26	342.19166
A	MT-1-n2-03.tif	DB	I=I(1:600,201:800);	0.16	
B	MT1-31.jpg	DB	I=I(1001:1600,1001:1600);	0.28	755.4268
B	MT-1-n3-10.tif	DB	I=I(1:600,1:600);	0.17	
C	MT1-HOSTROCK1. (between band).jpg	Between DB	I=I(1:400,301:700);	0.31	1573.3629
C	MT-1-n4-18.tif	Between DB	I=I(1:600, 1:600);	0.13	
D	MT1-7.jpg	DB	I=I(401:1000,1001:1600);	0.26	499.13381
D	MT-1-n5-14.tif	DB	I=I(1:600,151:750);	0.18	
E	MT1-35.jpg	DB	I=I(601:1200, 601:1200);	0.20	463.10549
E	MT-1-n6-20.tif	DB	I=I(1:600, 301:900);	0.16	
F	MT2-2.jpg	DB	I=I(201:700,1001:1500);	0.28	507.60169
F	MT-2-n1-22.tif	DB	I=I(1:600, 1:600);	0.17	
G	MT2-17.jpg	Between DB	I=I(301:800,1:500);	0.31	1039.4211
G	MT-2-n3-30.tif	Between DB	I=I(1:600,401:1000);	0.25	
H	MT2-23.jpg	DB	I=I(1201:1800,501:1100);	0.24	580.34459
H	MT-2-n4-33.tif	DB	I=I(1:600, 1:600);	0.16	
I	MT2-14.jpg	DB	I=I(1201:1800,1501:2100);	0.25	895.69468
I	MT-2-n5-35.tif	DB	I=I(1:600, 1:600);	0.16	
J	MT1-HOSTROCK2-4X.jpg	HR	I=I(1:400,851:1250);	0.32	2007.4558
J	MT-1-n1-outside band-06.tif	HR	I=I(1:600,101:700);	0.24	
K	MT1-9.jpg	DB	I=I(201:600,801:1200);	0.26	
L	MT1-13.jpg	DB	I=I(1:600,401:1000);	0.27	
M	MT1-33.jpg	DB	I=I(1001:1400,1501:1900);	0.28	
N	MT1-38.jpg	DB	I=I(301:900,401:1000);	0.29	
O	MT2-7.jpg	DB	I=I(1:600,601:1200);	0.28	
P	MT2-10.jpg	DB	I=I(601:1200,1001:1600);	0.25	
Q	MT2-15.jpg	DB	I=I(801:1400,1001:1600);	0.27	
R	MT2-16.jpg	DB	I=I(801:1400,1001:1600);	0.20	
S	MT2-21- 4x.jpg	HR	I=I(201:800,251:850);	0.35	
T	MT1-11 NARROW BETWEEN DB.jpg	Between DB	I=I(801:1400,1001:1600);	0.31	

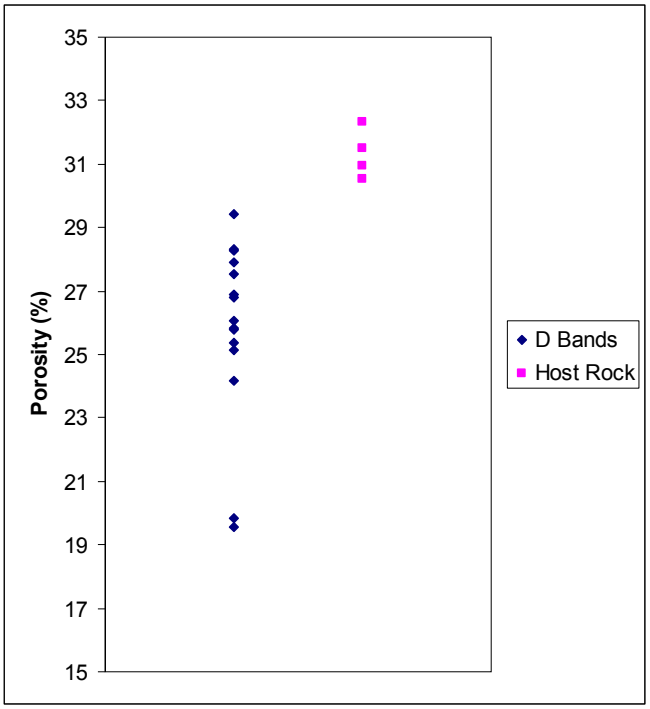

Figure 5-20: Porosity variation for selected areas on deformation bands and host rock: Porosity in host rock is higher than porosity in deformation bands and not varying too much (30% to 33%). In deformation bands we have wide range of porosity (19% to 30%) but all less than host rock which is in agreement with cataclastic bands.

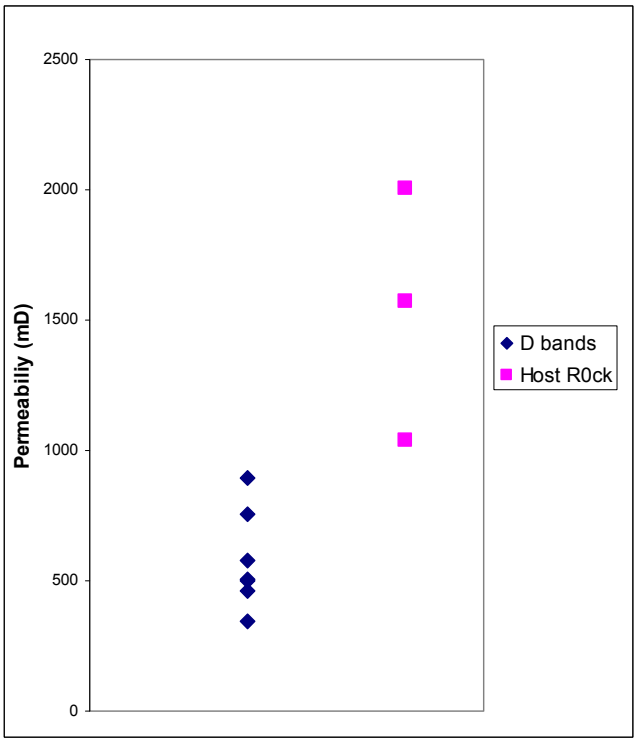

Figure 5-21: Permeability range for deformation bands and host rock: permeability in host rock is higher than deformation bands varying from 1500 mD to 2000 mD. In deformation bands we have permeability range from 350mD to 900 mD.

6 Discussions and Conclusions

This study was performed on a sample with cataclastic bands which are typically formed by grain crushing and fracturing within porous sandstone. Based on available studies (e. g. Antonellini & Aydin, 1994 and Torabi et al, in press) they have higher density and lower porosity & permeability compared to the host rocks resulting in change of fluid flow pattern in the sample.

Gamma-Ray measurement

According to Gamma-Ray scanning, the bands in the sample are denser than the host rock and it was expected that estimated porosity and consequently permeability in bands to be lower than the surrounding un-deformed rocks, this is also confirmed by the results of image processing (see **Microscopic studies**, in the discussion below)

.

Indirect porosity measurement

Porosity of the whole sample is estimated as 25% in one phase experiment and 21% in two phase experiments. This difference could be because of change in the sample properties during many injections, remaining some brine in the sample or measurement's errors. It should be noted that the experimental porosity was calculated indirectly, so they could not be very accurate, whereas estimated porosities using image processing shows higher magnitudes (30-33%).

Effect of deformation bands on fluid flow in miscible displacement

Figures 6-1 to 6-5 illustrate progressive movement of fluid front in the sample (light yellow to dark green) during different experiment and show how the deformation bands influence fluid pass in each flood of miscible displacement experiment.

In the first flood (Figure 6-1), we see further propagation of fluid from left to right of the sample because of the configuration of inlet #1 and outlet #3, but it cannot totally cover the right part of the sample. It seems that deformation bands affect the flow, especially in right-lower part of images. They do not allow the fluid to pass and reach directly the exit valve. The NaI enters the bottom groove and then exit from valve#3 (Figure 6-1).

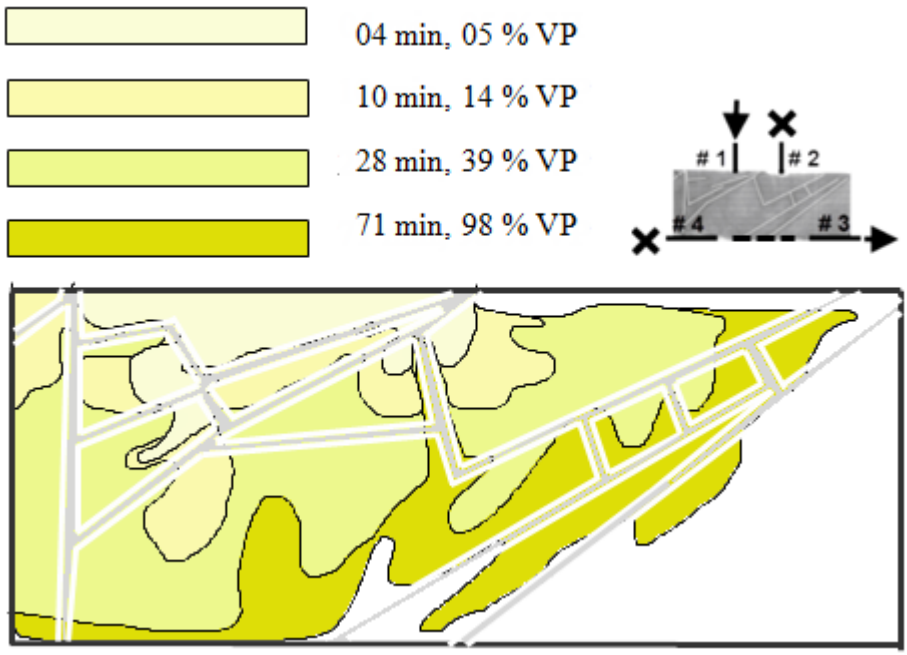

Figure 6-1: Flood 1 (miscible displacement), density: 70 g/l, rate: 15 ml/h, time: 79 min

In flood 2 (Figure 6-2), because of closeness of inlet #2 and outlet #3, the fluid directly moves toward the right part of the sample and has no chance to reach the left part of the sample. We can observe that deformation bands resist fluid pass and delay it.

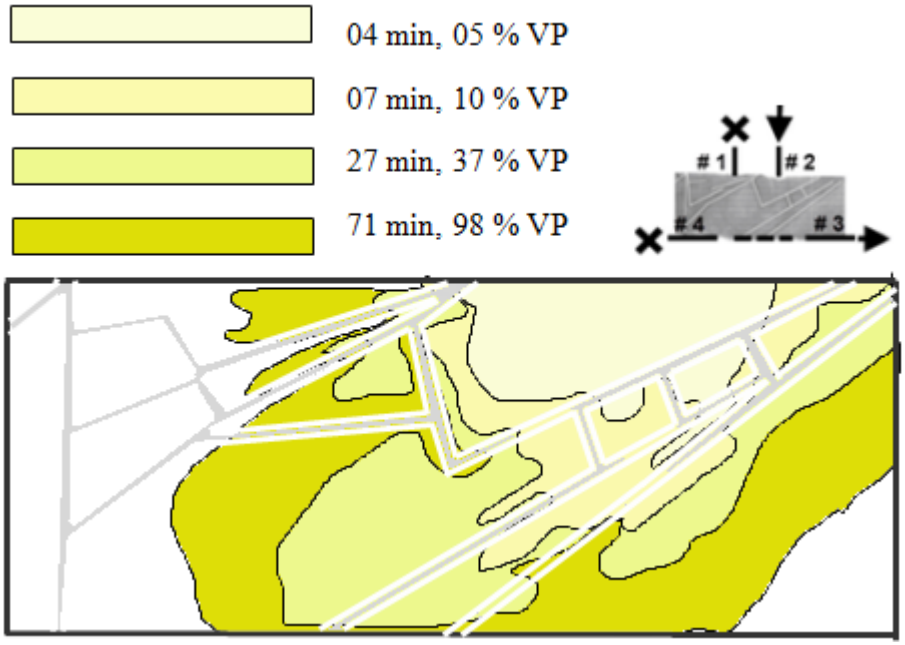

Figure 6-2: Flood 2 (miscible displacement), density: 70 g/l, rate: 15 ml/h, time: 84 min

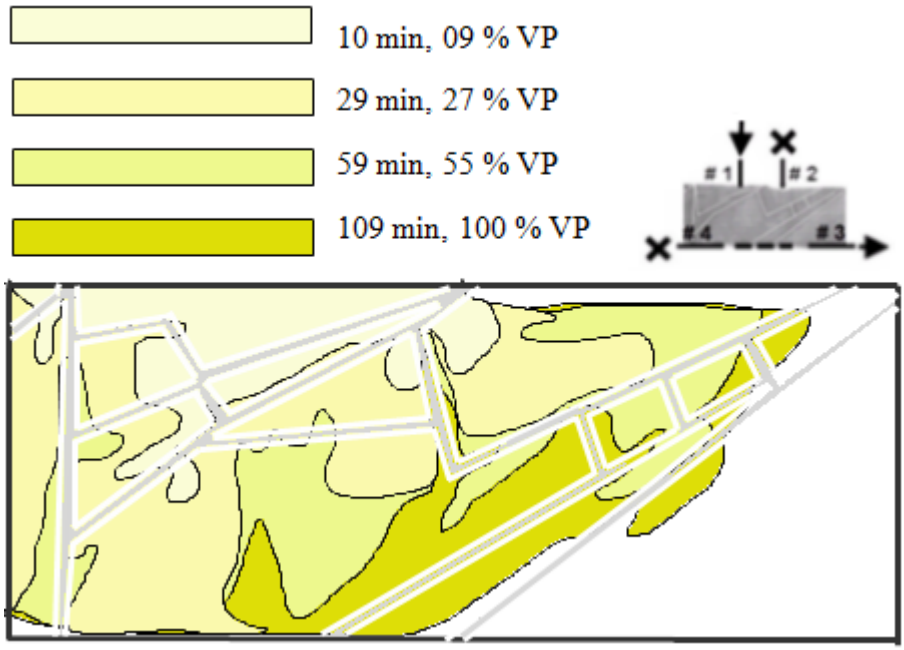

Figure 6-3: Flood 3 (miscible displacement), density: 100 g/l, rate: 10 ml/h, time: 118 min

The detail of fluid pattern varies from flood 1 to flood 3; due to the change of rate of injection in these two experiments. In the flood 3 (Figure 6-3) with longer time and lower rate, fluid has penetrated large areas in the beginning of the experiment.

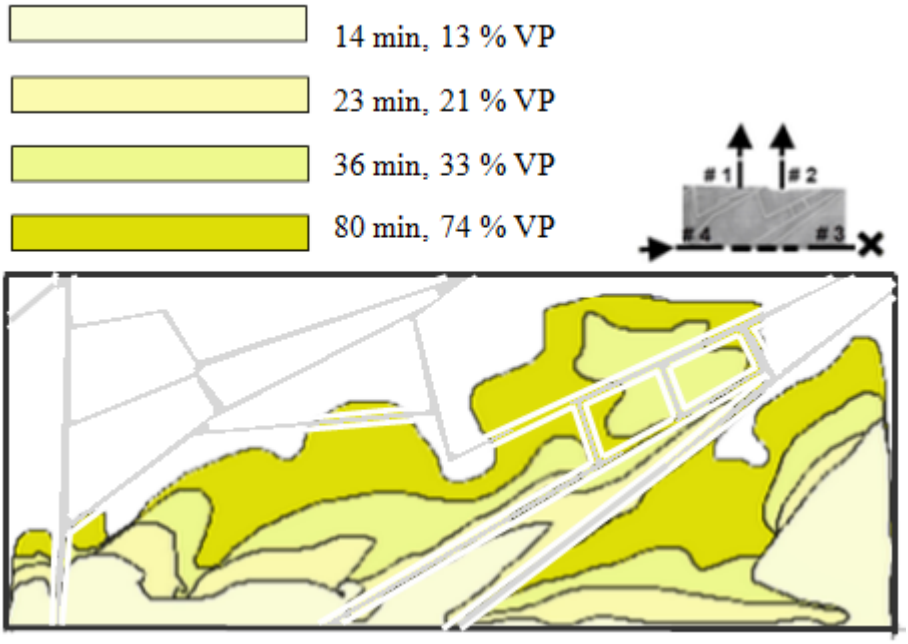

Figure 6-4: Flood 4 (miscible displacement), density: 100 g/l, rate: 10 ml/h, time: 80 min

The only difference between flood 4 and 5 is configuration of outlets (Figures 6-4 and 6-5). In flood 4 that has two outlets the fluid has chosen to move toward the more permeable part of

the sample, which is around outlet #2. This is confirmed by the result of thin section study that shows higher porosity and permeability close to outlet #2 than those deformation band intersections close to outlet #1. However, in flood 5 (Figure 6-5) the fluid has less chance to move toward outlet #2 as it is closed and therefore prefers to penetrate toward the left part of sample.

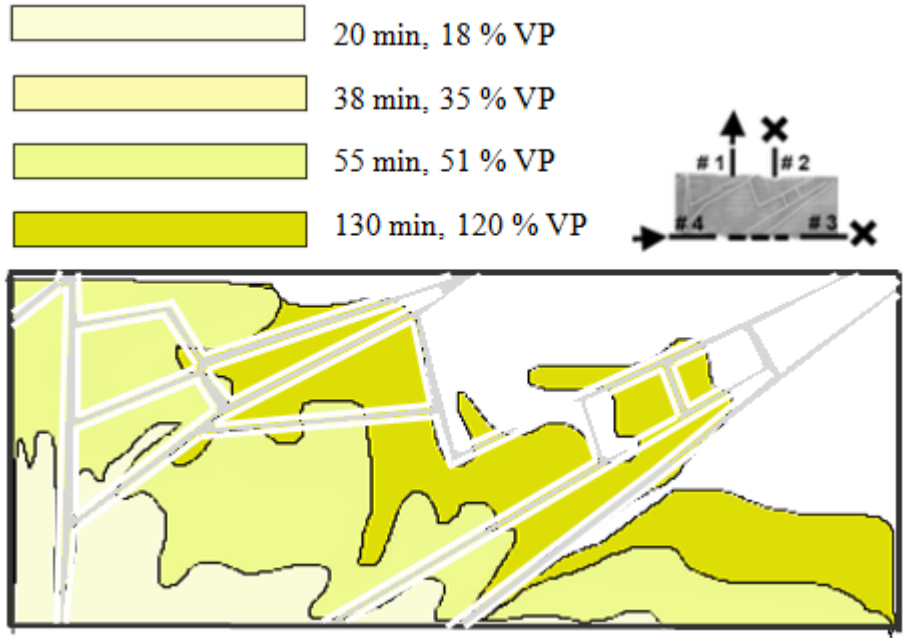

Figure 6-5: Flood 5 (miscible displacement), density: 100 g/l, rate: 10 ml/h, time: 127 min

By studying the presented figures (Figures 6-1 to 6-5), we conclude that deformation bands affect fluid flow pattern in the sample. They hinder flow across them, while they redirect the flow along themselves. In the absence of deformation bands we expect an even distribution of flow in sample radiating from inlet and exiting from outlet, while, in this deformed sample, deformation bands impact connectivity & increase tortuosity by redirecting fluid.

Effect of deformation bands on fluid flow in immiscible displacement

In the two phase experiments (figures 6-6 & 6-7), the extension of propagation of fluid front in the flood 4 could be related to different inlet configuration and also to the longer duration of injection during this experiment. The result of the two phase experiment when draining the brine by oil shows that oil does not completely replace the brine and only 45% of brine was replaced by oil. This could be related to the capillary effect induced by presence of deformation bands. A single band seems to increase capillary pressure between brine and oil.

Considering a reservoir with a number of clusters of deformation bands, this effect will increase capillary pressure in the reservoir and the fluid flow can be influenced.

Behaviour of sample in the two phase experiments shows that the sample is water (NaI) wet where the water phase saturation is higher than oil (Decane) phase.

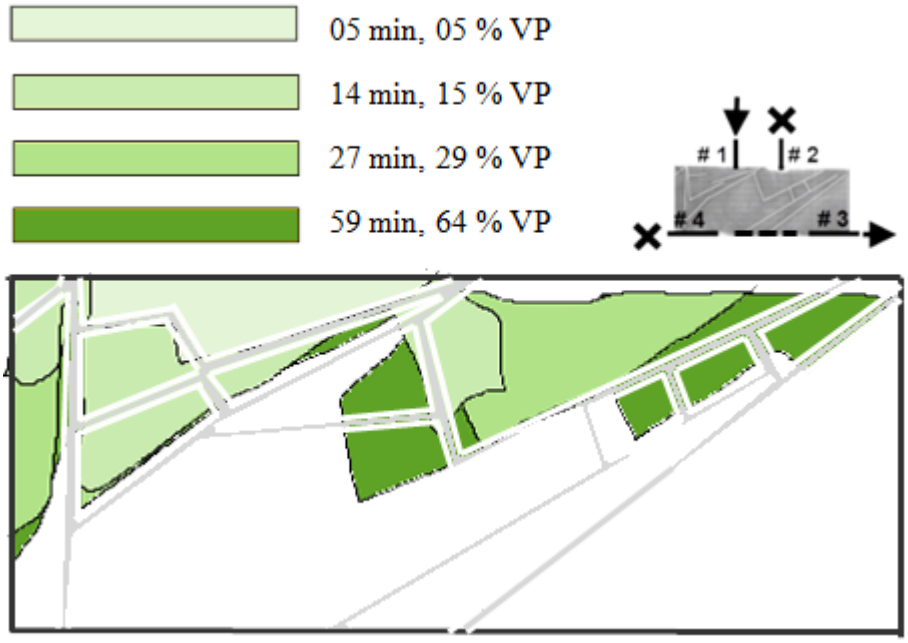

Figure 6-6: Flood 3 (two phase), density: rate: 10 ml/h, time: 59 min

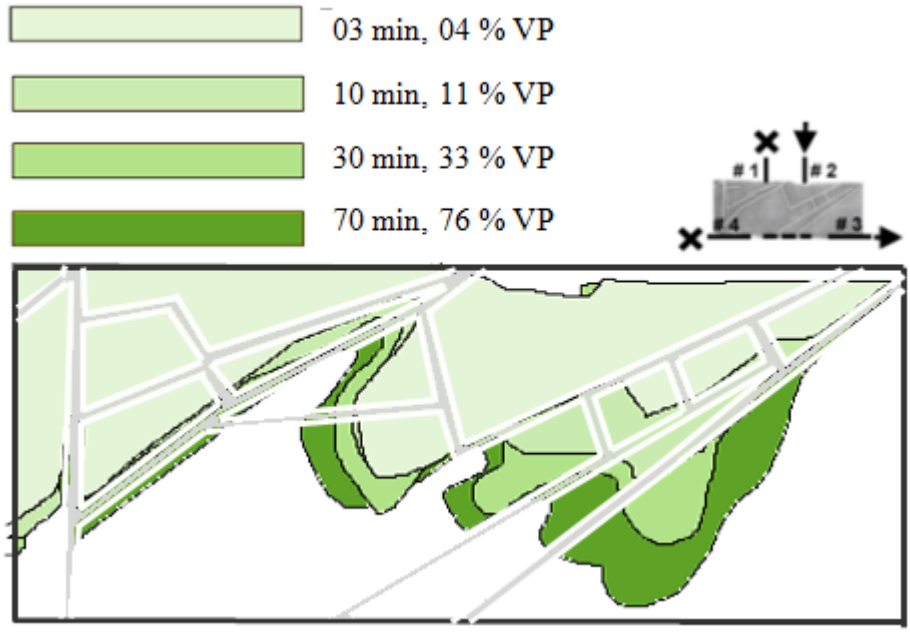

Figure 6-7: Flood 4 (two phase), density: rate: 10 ml/h, time: 79 min

Microscopic studies

The porosity estimated from image processing is in the range of 19% - 29% for deformation bands and 30% - 33% for the host rock. Optical images have been used for porosity measurements and the reason is that these images include larger and a more representative areas that contain more sufficient number of pores and grains (Torabi et al., 2008). Estimated permeability for deformation bands are between 350 mD and 900 mD and for host rock is between 1500 mD and 2000 mD. Porosity and permeability estimated from image processing are in agreement with the experimental results and former works (e. g. Torabi et al, in press, Torabi & Fossen 2009 and Antonellini & Aydin, 1994) indicating lower porosity and permeability in deformation bands comparing to host rock.

The porosity and permeability estimated for deformation bands based on image processing are slightly higher compared to similar studies on cataclastic bands. Antonellini & Aydin, 1994 reported extremely variable two dimensional porosity range of 1% to 18% for the samples from (Entrada sandstone) using video-image analysis and point counting of thin sections. Furthermore, newer study performed by Torabi & Fossen in 2009 using the same image processing technique as this work shows estimated range of 12% to 32% for porosity of deformation bands. However, the degree of cataclasis is an important factor that influences the estimated porosity and permeability values (Torabi and Fossen, 2009). The higher porosity and permeability values estimated for our samples could be related to a mild cataclasis in the studied deformation bands.

Regardless of the location for selected areas (deformation band or host rock) on the images, porosity–permeability relation shown in Figure 6-8 is in agreement with results published by Torabi and Fossen in 2009 (samples with cataclastic bands). This consistency is even better for the results published by Torabi et al (in press) for undeforemd silty sandstone.

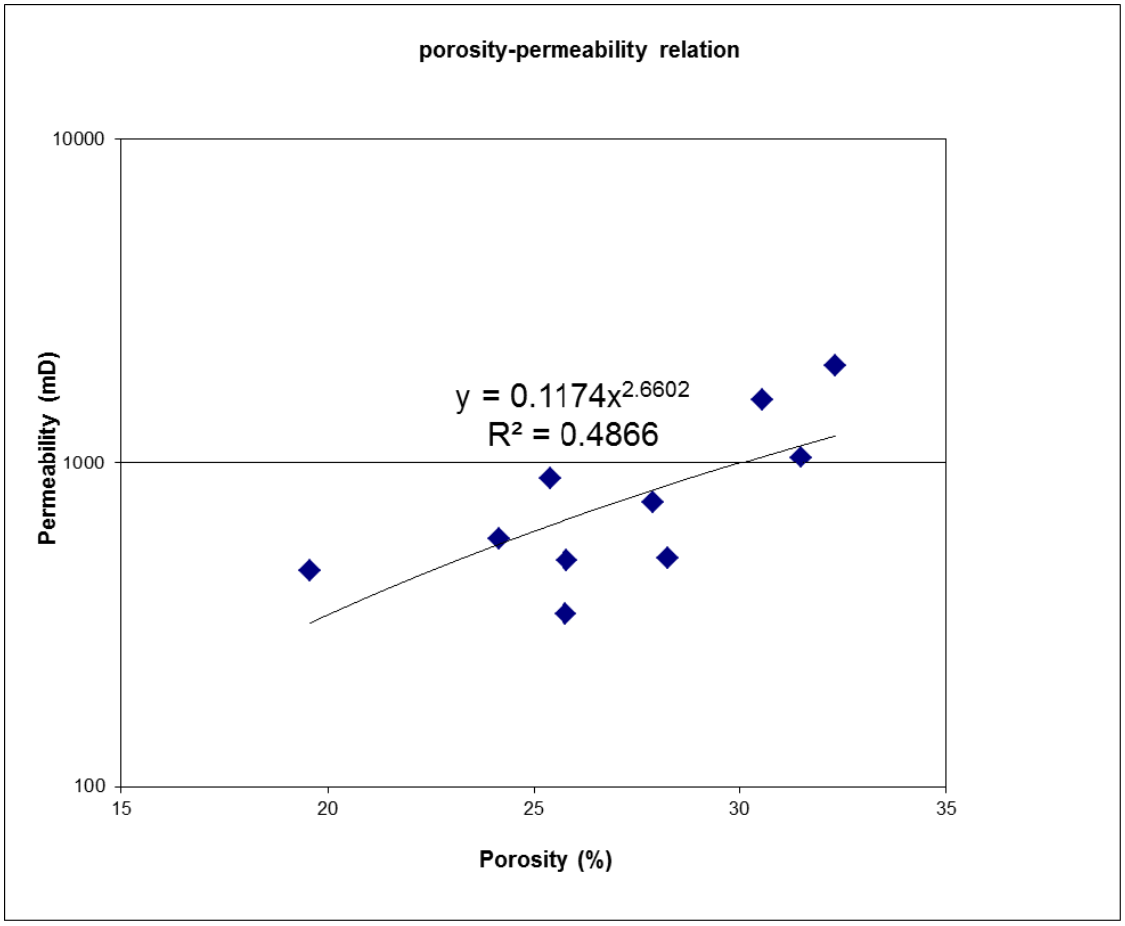

Figure 6-8: Porosity and permeability relation: general trend agrees increase of permeability for higher magnitude of porosity, but it is not necessarily correct for all data.

Effect on hydrocarbon recovery

Cataclastic deformation bands locally redirect and delay fluid pass; however it is observed in some of the floods, where we use longer injection time that the fluid passes almost completely through the deformation bands and therefore we can conclude that single bands or small cluster of them may not have significant global effect on hydrocarbon recovery. This result is in agreement with the previous studies (e. g. Ersland, G., et al, 2010). This behaviour should be due to rapid variations in properties along bands even in millimeter and centimeter scale that make them leaky (Torabi & Fossen, 2009) and also due to conduit behaviour parallel to bands which is observed in some of the floods in these experiments. The anisotropy in permeability induced by deformation bands has been reported previously (Torabi et al, 2008 and Antonellini & Aydin, 1994) as change in permeability of cataclastic deformation bands measured parallel and perpendicular to bands.

However, the total effective permeability of the reservoir can be reduced due to heterogeneities represented by deformation bands which increase the sinuosity and tortuosity of fluid flow. This could have implications for several applications such as well planning, field development of reservoirs, and CO2 storage underground, where deformation bands could impact the total capacity of the reservoir.

Further work

We recommend applying the similar experiment of flow visualization on more samples with other types of deformation bands from different locations that would make it easier to compare and calibrate the data versus pervious works.

Next proposal is doing two phase experiment (the same as conducted here) just on the host rock and compare it with deformed sample. This would help us to judge about the capillary effect induced by the bands.

It is also suggested to simulate the fluid flow through deformation bands using commercial software for a sample which has been imaged (X-Ray) under fluid flow experiment and its properties (porosity and permeability) have been estimated using BSE images.

7 References

1) **Archie, G.E.**, The Electrical Resistivity Log as an Aid in Determining Some Reservoir Characteristics,Trans AIME, 146: p. 54 – 67, 1942.

2) **Aydin, Atilla.** Small faults formed as deformation bands in sandstone, Pure and Applied Geophysics, v. 116, 1978.

3) **Aydin, A., Borja, R.I., Eichhuble, P.**, Geological and mathematical framework for failure modes in granular rock, Journal of structural geology, 2006.

4) **Antonellini, Marco & Aydin, Atilla.**, Effect of faulting on fluid flow in porous sandstone: petrophysical properties, AAPG Bulletin, v. 78, no. 3, 1994.

5) **Berg, S.S., Øian, E., Skar, T. & Gabrielsen, R.H.**,The architecture of faults and its consequence for fluid flow. Geologiska Föreningens I Stockholms Förhandlingar 126, 61-62, 2004.

6) **Berg S. S. and Skar T**., Controls on damage zone asymmetry of a normal fault zone: outcrop analyses of a segment of the Moab fault, SE Utah, Journal of Structural Geology 27, 2005

7) **Bernabe, Y. & Brace, W.F.**, Deformation and fracture of Berea sandstone. In: Duba, A.G., Durham, W.B., Handin, J.W. & Wang, H.F. (eds) The Brittle–Ductile Transition in Rocks. Geophysical Monograph, American Geophysical Union, 56, 91–101, 1990.

8) **Berryman, J. G.**, Planar spatial correlations, anisotropy, and specific surface area of stationary random porous media: Journal of Applied Physics, v. 83, p. 1685–1693, doi:10.1063/1.366885, 1998.

9) **Blair, S. C., P. A. Berge, and J. G. Berryman.**, Using two-point correlation functions to characterize microgeometry and estimate permeabilities of sandstones and porous glass: Journal of Geophysical Research, v. 101, p. 20,359–20, 375, 1996.

10) **Brace, W. E.**, Permeability from resistivity and pore shape: Journal of Geophysical Research, v. 82, p. 3343–3349, doi:10.1029/JB082i023p03343, 1977.

11) **Brown, N., Ducket, R.A., Ward, I.M.**, Deformation bands in polyethylene therephthalate, British Journal of applied physics, 1968.

12) **Du Bernard, X. D., Eichhubl, P., & Aydin, A.**, Dilation bands: A new form of localized failure in granular media, Geophysical Research Letters, 2002.

13) **Ellingsen, Einar.**, Interaction of Diagenesis and Deformation of Faulted Sandstone Reservoirs, Master of Science Thesis in Petroleum Geology, Department of Earth Science, University of Bergen, 2011

14) **Ersland, G., et al**, Impact of Deformation Bands on Fluid Flow and Oil Recovery, International Symposium of the Society of Core Analysts held in Halifax, Nova Scotia, Canada, 4-7 October, 2010.

15) **Fisher, Q.J., Knipe, R.J.**, The permeability of faults within siliciclastic petroleum reservoirs of the North sea and Norwegian continental shelf, Marin and Petroleum Geology, 2001.

16) **Fossen, Haakon & Hesthammer, Jonny.** Deformation bands and their significance in porous sandstone reservoirs, EAGE, 1998.

17) **Fossen, H., Schultz, R. A., Shipton Z.K. & Mair, K.**, Deformation bands in sandstone: a review, Journal of Geological Society (London), Vol. 164, 2007.

18) **Gabrielsen, R.H., Koestler, A.G.**, Description and structural implications of fractures in late Jurassic sandstone of the Troll field, Norsk Geologisk Tidsskrift ,1987.

19) **Gibson, Richard G.**, Physical character and fluid-flow properties of sandstone-derived fault zones, Geological Society (London) Special Publication127, 1998.

20) **Holcomb, D.J. & Olsson, W.A.**, Compaction localization and fluid flow, Journal of Geophysical Research, 108(B6), 2290, 2003.

21) **Horgen, Thorbjørn.**, An Experimental Study of Unstable Miscible Displacement in Vuggy Carbonate and Sandstone, 2010.

22) **Jamison, W.R., Stearns, D.W.**, Tectonic deformation of Wingate sandstone, Colorado National Monument, AAPG, 1982.

23) **Johansen, T.E.S., Fossen, H. & Kluge, R.**,The impact of syn-kinematic porosity reduction on damage zone architecture in porous sandstone; an outcrop example from the Moab Fault, Utah. Journal of Structural Geology, 27, 1469–1485, 2005.

24) **Jolley S. J., H. Dijk, J. H. Lamens, Q. J. Fisher, T. Manzocchi ,H. Eikmans and Y. Huang,** Faulting and fault sealing in production simulation models:Brent Province, Northern North Sea, Petroleum Geoscience, Vol. 13, pp. 321–340, 2007.

25) **Kolyukhin D. and Torabi A.**, Statistical analysis of the relationships between faults attributes, J. Geophys. Res., 117, 2012

26) **Leveille, G.P. et al**, Compartmentalization of rotliegendes gas reservoirs by sealing faults, Geological Society (London), 1997.

27) **Manzzochi, T., Walsh, J.J., Bailey, W.R.**, Population scaling biases in map samples of power law fault systems. Journal of Structural Geology 31,1612e1626, 2009.

28) **Noremark, Bjørn.** Experimental Study of Viscous Fingering in Miscible Displacements, 2010.

29) **Ogilvie, S.R. & Glover, P.W.J.**, The petrophysical properties of deformation bands in relation to their microstructure, Earth Planet. Sci. Lett., 193 (1-2), 129-142, 2001.

30) **Parry, W.T., Chan, M.A. & Beitler, B.**, Chemical bleaching indicates episodes of fluid flow in deformation bands in sandstone. AAPG Bulletin, 88, 175–191, 2004.

31) **Rykkelid, E. Fossen, H.**, Layer rotation around vertical fault overlap zones: observations from seismic data, field examples and physical experiments, Marine and Petroleum Geology 19, 181-192, 2002.

32) **Sample, J.C., Woods, S., Bender, E. & Loveall, M.**, Relationship between deformation bands and petroleum migration in an exhumed reservoir rock,Los Angeles Basin, California, USA. Geofluids, 6, 105–112, 2006.

33) **Sen, P. N., C. Scala, and M. H. Cohen.**, 1981, A self-similar model for sedimentary rocks with application to the dielectric constant of fused glass beads: Geophysics, v. 46, p. 781–795, doi:10.1190/1.1441215, 1981.

34) **Sigda, J., Wilson, J.L.**, Are faults preferential flow paths through semi-arid and arid vadose zones?: Water Resources Research, v. 39, doi:10.1029/2002WR001406¸ 2003.

35) **Shipton, Z.K, Cowie, P.A.**, A conceptual model for the origin of fault damage zone structures in high-porosity sandstone.Journal of Structural Geology 25, 333– 344 (erratum, Journal of Structural Geology 25, 1343–1345), 2003.

36) **Torabi, Anita & Fossen, Haakon.**, Spatial variation of microstructure and petrophysical properties along deformation bands in reservoir sandstones, AAPG Bulletin, v. 93, no. 7, 2009.

37) **Torabi, A., Berg, S. S.**, Scaling of fault attributes; a review, Marine and Petroleum Geology, v. 28, 8, p. 1444-1460, 2011.

38) **Torabi, A., Fossen, H., Braathen A.**, Insight into petrophysical properties of deformed sandstone reservoirs. AAPG Bulletin, in press.

39) **Torabi, A., Fossen, H., Alaei B.**, Application of spatial correlation functions in permeability estimation of deformation bands in porous rocks, J. Geophys. Res., 113, 2008.

40) **Torabi, A.**, Deformation bands in porous sandstones, their microstructure and petrophisical properties, PhD thesis, UiB, ISBN 978-82-308-0528-2, 2008.

41) **Wong, P. Z., J. Koplik, and J. P. Tomanic.**, Conductivity and permeability of rocks: Physics Review, v. 30, p. 6606–6614, 1984.

8 Appendix

Appendix includes all the X-Ray images from floods in one phase and two phases, the movies showing the fluid flow in experiments and optical and BSE images used for estimation of porosity and permeability, copied on CD enclosed to this thesis.